2014

Type I interferon responses in rhesus macaques prevent SIV infection and slow disease progression

Netanya G. Sandler
National Institutes of Health

Steven E. Bosinger
Yerkes National Primate Research Center, steven.bosinger@emory.edu

Jacob D. Estes
Frederick National Laboratory, estesj@mail.nih.gov

Richard T. R. Zhu
National Institutes of Health

Gregory K. Tharp
Yerkes National Primate Research Center

See next page for additional authors

Authors
Netanya G. Sandler, Steven E. Bosinger, Jacob D. Estes, Richard T. R. Zhu, Gregory K. Tharp, Eli Boritz, Doron Levin, Sathi Wijeyesinghe, Krystelle Nganou Makamdop, Gregory D. del Prete, Brenna J. Hill, J. Katherina Timmer, Emma Reiss, Ganit Yarden, Samuel Darko, Eduardo Contijoch, John Paul Todd, Guido Silvestri, Martha Nason, Robert B. Norgren Jr., Brandon F. Keele, Srinivas Rao, Jerome A. Langer, Jeffrey D. Lifson, Gideon Schreiber, and Daniel C. Douek

LETTER

doi:10.1038/nature13554

Type I interferon responses in rhesus macaques prevent SIV infection and slow disease progression

Netanya G. Sandler[1]†, Steven E. Bosinger[2,3], Jacob D. Estes[4], Richard T. R. Zhu[1], Gregory K. Tharp[2,3], Eli Boritz[1], Doron Levin[5], Sathi Wijeyesinghe[1], Krystelle Nganou Makamdop[1], Gregory Q. del Prete[4], Brenna J. Hill[1], J. Katherina Timmer[1], Emma Reiss[1], Ganit Yarden[5], Samuel Darko[1], Eduardo Contijoch[1], John Paul Todd[6], Guido Silvestri[2], Martha Nason[7], Robert B. Norgren Jr[8], Brandon F. Keele[4], Srinivas Rao[6], Jerome A. Langer[9], Jeffrey D. Lifson[4], Gideon Schreiber[5] & Daniel C. Douek[1]

Inflammation in HIV infection is predictive of non-AIDS morbidity and death[1], higher set point plasma virus load[2] and virus acquisition[3]; thus, therapeutic agents are in development to reduce its causes and consequences. However, inflammation may simultaneously confer both detrimental and beneficial effects. This dichotomy is particularly applicable to type I interferons (IFN-I) which, while contributing to innate control of infection[4–10], also provide target cells for the virus during acute infection, impair CD4 T-cell recovery, and are associated with disease progression[6,7,11–19]. Here we manipulated IFN-I signalling in rhesus macaques (*Macaca mulatta*) during simian immunodeficiency virus (SIV) transmission and acute infection with two complementary *in vivo* interventions. We show that blockade of the IFN-I receptor caused reduced antiviral gene expression, increased SIV reservoir size and accelerated CD4 T-cell depletion with progression to AIDS despite decreased T-cell activation. In contrast, IFN-α2a administration initially upregulated expression of antiviral genes and prevented systemic infection. However, continued IFN-α2a treatment induced IFN-I desensitization and decreased antiviral gene expression, enabling infection with increased SIV reservoir size and accelerated CD4 T-cell loss. Thus, the timing of IFN-induced innate responses in acute SIV infection profoundly affects overall disease course and outweighs the detrimental consequences of increased immune activation. Yet, the clinical consequences of manipulation of IFN signalling are difficult to predict *in vivo* and therapeutic interventions in human studies should be approached with caution.

We designed and produced an IFN-I receptor antagonist (IFN-1ant) that blocks IFN-α2 antiviral and antiproliferative activity *in vitro*[19]. Six rhesus macaques received 1 mg of IFN-1ant daily for 4 weeks following intrarectal challenge with SIV_{MAC251} (dosage based on previous dose–response studies; Extended Data Fig. 1a–d); nine macaques received saline (Extended Data Fig. 1e). Initial assessment of *in vivo* effects revealed delayed peak mRNA expression of *MX1* and *OAS2* in the IFN-1ant macaques (Extended Data Fig. 2a, b), but peak expression levels did not differ between cohorts. Whole-transcriptome sequencing revealed that expression of most interferon-stimulated genes (ISGs) in peripheral blood mononuclear cells (PBMCs) was significantly decreased at 7 days post-infection (d.p.i.) in the IFN-1ant-treated compared to placebo-treated macaques (Fig. 1a), including the antiviral genes *APOBEC3G* and *MX2*, those that code for cyclic GMP-AMP synthase (cGAS) and tetherin[4,5,20], and *IRF7*, a master IFN-I signalling inducer[21], indicating profound disruption of IFN-I signalling (Fig. 1b). Most ISGs in the IFN-1ant group normalized at 10 and 21 d.p.i. and were upregulated at 28 and 84 d.p.i. (Extended Data Fig. 2c). Consistent with transcriptional data (Extended Data Fig. 2d, e), APOBEC3G, TRIM5α and MX2 protein expression by quantitative immunohistochemistry was significantly attenuated in lymph nodes at 4 weeks post-infection (w.p.i.) compared to placebo (Fig. 1c). Thus, IFN-1ant treatment during acute SIV infection resulted in delayed and decreased antiviral gene and protein expression in peripheral blood and lymph nodes.

Consistent with reduced antiviral gene expression, IFN-1ant macaques had significantly higher plasma viral loads (pVLs) than placebo macaques during acute infection (Fig. 2a) and after 20 w.p.i. despite similar numbers of transmitted/founder viruses (measured 10 d.p.i., Extended Data Fig. 8a). Delayed peak ISG expression, however, was predictive of higher pVLs at peak and 12 w.p.i. and higher PBMC-associated SIV *gag* DNA levels at 28 d.p.i. (Extended Data Fig. 2f–h). Additionally, the number of lymph node SIV RNA^+ cells per mm^2 as determined by *in situ* hybridization was significantly higher in macaques treated with IFN-1ant compared to placebo during chronic infection (Fig. 2b). Thus, early IFN-I signalling was critical for early and long-term control of SIV replication and virus reservoir size.

Although both groups experienced a similar, significant decrease in circulating CD4 T-cell frequency (Fig. 2c) and CD4/CD8 T-cell ratio (Extended Data Fig. 3a) between 0 and 12 w.p.i., IFN-1ant macaques experienced a profound decline with a lower lymph node CD4 T-cell frequency and CD4/CD8 T-cell ratio beyond 12 w.p.i. (Fig. 2d and Extended Data Fig. 3b). The frequency of $CCR5^+$ memory CD4 T cells, potential targets for infection, was significantly lower in blood in IFN-1ant-treated than placebo-treated rhesus macaques through 12 w.p.i. (Fig. 2e), and lymph nodes at 4 and >12 w.p.i. (Fig. 2f), suggesting depletion due to infection. Circulating T-cell activation, reflected by HLA-DR^+ and $Ki67^+$ memory CD4 and CD8 T-cell frequencies, was not significantly different between groups at 4 or >12 w.p.i. (Supplementary Information). However, HLA-DR^+ and $Ki67^+$ memory CD4 and CD8 T-cell frequencies were significantly lower in the lymph nodes of IFN-1ant macaques than placebo at >12 w.p.i. (Extended Data Fig. 3c–f). Taken together, IFN-I signalling blockade during acute SIV infection resulted in attenuated T-cell activation in lymphoid tissue yet accelerated CD4 T-cell depletion.

Clinical outcome ultimately gives the most comprehensive measure of disease state. Consistent with a median life expectancy of 1 year[22], the six placebo-treated macaques followed through 44 w.p.i. (three were transferred to another study before 30 w.p.i.) lived, but the IFN-1ant macaques began dying of AIDS at 24 w.p.i. and all were euthanized per protocol for signs of AIDS by 30 w.p.i. (Fig. 2g). Thus, blocking IFN-I signalling during only the first 4 weeks of infection resulted in accelerated disease progression and death from AIDS.

Exploration of the molecular mechanisms underlying the accelerated disease progression by whole-transcriptome sequencing revealed statistically

[1]Human Immunology Section, Vaccine Research Center, National Institute of Allergy and Infectious Disease, National Institutes of Health, Bethesda, Maryland 20892, USA. [2]Division of Microbiology and Immunology, Emory Vaccine Center, Yerkes National Primate Research Center, Atlanta, Georgia 30322, USA. [3]Non-Human Primate Genomics Core, Yerkes National Primate Research Center, Robert W. Woodruff Health Sciences Center, Emory University, Atlanta, Georgia 30322, USA. [4]AIDS and Cancer Virus Program, Leidos Biomedical Research, Inc., Frederick National Laboratory, Frederick, Maryland 21702, USA. [5]Department of Biological Chemistry, Weizmann Institute of Science, Rehovot 76100, Israel. [6]Laboratory of Animal Medicine, Vaccine Research Center, National Institute of Allergy and Infectious Disease, National Institutes of Health, Bethesda, Maryland 20892, USA. [7]Biostatistics Research Branch, Division of Clinical Research, National Institute of Allergy and Infectious Diseases, National Institutes of Health, Bethesda, Maryland 20892, USA. [8]Department of Genetics, Cell Biology and Anatomy, University of Nebraska Medical Center, Omaha, Nebraska 68198, USA. [9]Department of Pharmacology, Rutgers - Robert Wood Johnson Medical School, Piscataway, New Jersey 08854, USA. †Present address: Division of Infectious Diseases, Department of Internal Medicine, University of Texas Medical Branch at Galveston, Galveston, Texas 77555, USA.

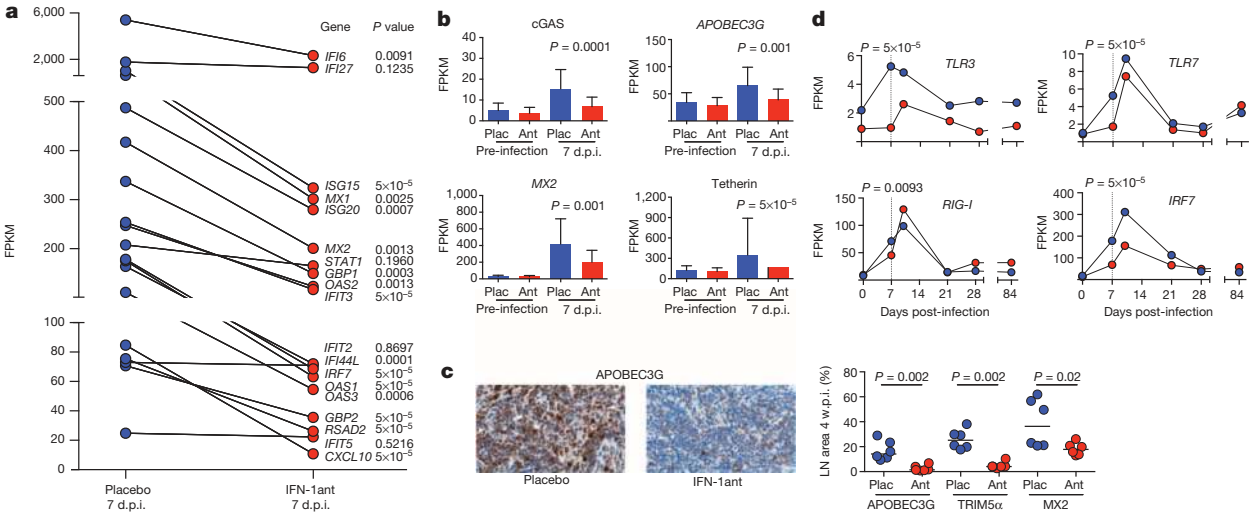

Figure 1 | IFN-1ant suppresses early antiviral responses. **a**, Expression of ISGs in macaques treated with IFN-1ant ($n = 6$) or placebo saline ($n = 9$) 7 days after SIV infection. FPKM (log-transformed fragments per kilobase of transcript per million fragments sequenced) reflects the relative abundance of transcripts. *P* values indicate differentially expressed genes at 7 d.p.i. **b**, Expression assessed by RNA sequencing (RNA-seq) of antiviral genes *APOBEC3G*, *MX2* and those that code for cGAS and tetherin in PBMCs before and 7 days after SIV infection in macaques that received IFN-1ant (Ant, $n = 6$) or placebo (Plac, $n = 9$) injections. Error bars indicate range. *P* values were calculated by Mann–Whitney *U* test. **c**, APOBEC3G, TRIM5α and MX2 protein expression by immunohistochemistry of lymph nodes (LNs) at 4 w.p.i. in placebo ($n = 6$) and IFN-1ant ($n = 6$) macaques. Horizontal bars represent median values. *P* values were calculated by Mann–Whitney *U* test. The left panels are representative images of APOBEC3G staining from each group. **d**, Expression of genes involved in pattern recognition receptor signalling of IFN-1ant-treated ($n = 6$) macaques compared to placebo ($n = 9$). *P* values represent the differential expression between IFN-1ant and placebo macaques at 7 d.p.i. For all panels, IFN-1ant-treated macaques are represented in red, placebo-treated macaques in blue.

significant enrichment of pathways regulating innate immunity, IFN-I production and T- and B-lymphocyte activation (Extended Data Fig. 4a–c) with significant downregulation of most genes in the IFN-1ant group at 7 d.p.i. compared to placebo-treated controls (Fig. 1d and Extended Data Fig. 2c). Relative to placebo, the most significantly perturbed pathway in the IFN-1ant-treated animals consisted of pathogen-associated pattern recognition receptor (PRR) signalling molecules (Fig. 1d and Extended Data Fig. 4a), with significant downregulation of several viral PRRs (*TLR3*, *TLR7*, *DDX58/RIG-I*, *MDA5/IFIH1*) and their downstream adaptors (*TICAM1/TRIF*) or transcription factors (*IRF7*) in IFN-1ant macaques compared to placebo (Extended Data Fig. 4c). Concordantly, expression of the downstream mediators *IL-6*, *TNF* and *IL-1β* was significantly reduced.

Consistent with their responsiveness to IFN-I[23], the frequencies of total and cytotoxic $CD16^+$ natural killer (NK) cells were significantly lower in the IFN-1ant group than placebo at >12 w.p.i., although there were no diferences at 4 w.p.i. (Extended Data Fig. 3g–i). However, we observed no significant differences in phenotype, function or timing of CD4 or CD8 T-cell responses (Extended Data Fig. 5 and Supplementary Information).

Collectively, these data suggest that IFN-I signalling early in SIV infection is critical for innate immune control of virus replication and that its antagonism, even if only brief during the acute phase, results in decreased virus control, accelerated CD4 T-cell depletion and progression to AIDS.

Given these findings, we hypothesized that administering IFN-I could improve SIV_{MAC251} control despite evidence suggesting that inflammation exacerbates virus acquisition and disease progression[1–3,13]. Six macaques received 6 μg kg^{-1} pegylated IFN-α2a dosed weekly, as determined in prior studies[24], starting 1 week before challenge and continued through 4 weeks after systemic infection (defined as detectable pVL 7 days post-challenge). Macaques were followed until 12 w.p.i. then euthanized per protocol (Extended Data Fig. 1e). Whereas all nine placebo macaques were infected after the first intrarectal inoculation, IFN-α2a treatment significantly delayed systemic infection, necessitating two, three or five challenges to infect these macaques (Fig. 3a), and significantly decreased the number of transmitted/founder variants (Extended Data Fig. 8a). The macaques that required more challenges had fewer transmitted/founder variants (Fig. 3b); however, the circulating viruses at peak viral load in both groups were equally susceptible to *in vitro* IFNα inhibition (data not shown). Thus, treatment with IFN-α2a during SIV challenge increased host resistance to systemic infection.

We assessed whether ISGs may have contributed to resistance to infection. We found that *MX1* and *OAS2* gene expression detected by quantitative reverse transcription PCR (qRT–PCR) increased after one IFN-α2a dose but decreased after repeated administration, suggesting an IFN-desensitized state (Extended Data Fig. 6a–d) resulting in no significant differences between treated and placebo groups on the day of infectious challenge. Furthermore, IFN-α2a macaques had lower ISG expression compared to placebo at 7 and 10 d.p.i., including those encoding cGAS, APOBEC3G, MX2 and tetherin (Fig. 3c–f and Extended Data Fig. 7a–b). At 4 w.p.i., after 6, 7 or 9 doses of IFN-α2a, lymph node TRIM5α protein expression was significantly lower in the IFN-α2a group compared to placebo (Extended Data Fig. 8b). To explore the effects of IFN-α2a administration on ISG expression further, we performed whole-transcriptome sequencing on uninfected rhesus macaques administered pegylated IFN-α2a for 3 weeks. Seven days after one IFN-α2a dose, expression of virus restriction factors including *TRIM22*, *MX2* and *IRF7* was increased in PBMCs, lymph nodes and rectum (Extended Data Fig. 7c–h). However, after 3 doses these ISGs returned to pre-treatment expression levels (*MX2*) or lower (*TRIM22* and *IRF7*), consistent with the timing of infection of the SIV-challenged macaques. (Extended Data Fig. 7c–h). We found no *in vitro* IFN-neutralizing activity in the plasma at the time of infection to explain the loss of exogenous IFN-α2a activity (Extended Data Fig. 6e and Supplementary Information), suggesting that ISG downregulation probably occurred as a result of intrinsic regulatory mechanisms. Indeed, *FOXO3a*, a central regulator of IFN-I feedback[25], was significantly upregulated in the IFN-α2a compared to placebo macaques at 7 d.p.i. (Fig. 3g and Extended Data Fig. 6g) and, concordantly, ISGs demonstrated to be repressibly bound by FOXO3a (ref. 25) had lower expression at 7 d.p.i. (Extended Data Fig. 6h). We also assessed a broad panel of genes predicted to be bound by FOXO3a (ref. 25) using gene-set enrichment analysis and observed a significantly lower cumulative ranking of FOXO3a targets in the 7 d.p.i. IFN-α2a-treated macaque transcriptome data when contrasted to the 7 d.p.i. placebo data (Fig. 3h), suggesting increased FOXO3a-mediated repression in the IFN-α2a macaques. Indeed, after 21 days of

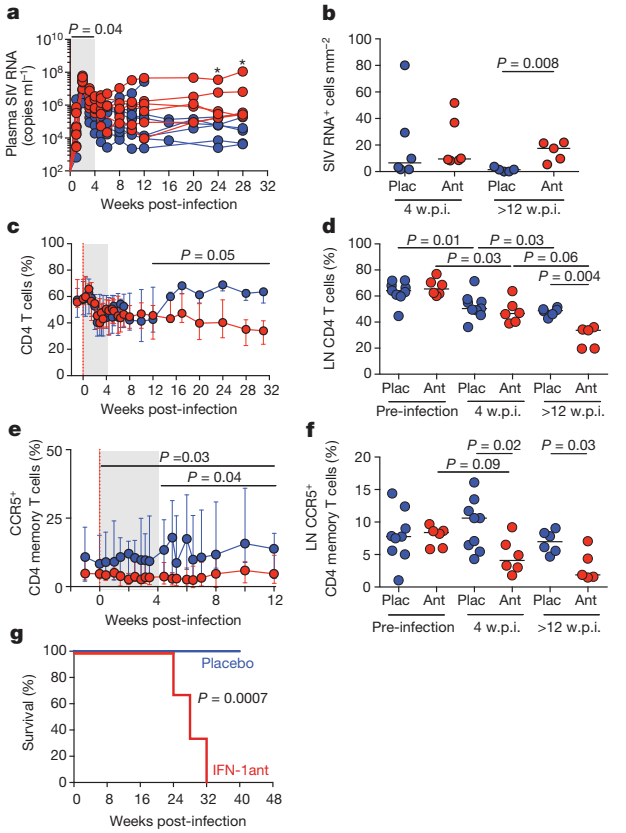

Figure 2 | IFN-1ant accelerates disease progression in SIV-infected rhesus macaques. **a**, Plasma SIV RNA levels during acute and chronic SIV infection in macaques treated with IFN-1ant ($n = 6$) or placebo saline ($n = 9$). *$P < 0.05$. Shading indicates treatment period. *P* value represents the comparison between groups of the areas under the curve (AUC) (0–4 w.p.i.). **b**, SIV RNA-containing cells in the lymph nodes by *in situ* hybridization at 4 and 12 w.p.i. in IFN-1ant (Ant, $n = 6$) and placebo (Plac, $n = 6$) macaques. Horizontal bars represent median values. *P* value was calculated by Mann–Whitney *U* test. **c**, Frequency of CD4 T cells in peripheral blood during acute and chronic SIV infection in macaques treated with IFN-1ant ($n = 6$) or placebo saline ($n = 9$). Error bars indicate range. Red vertical line indicates day 0 of systemic SIV infection. Shading indicates treatment period. *P* value represents the comparison between groups of the AUC (12-32 w.p.i.). **d**, Frequency of CD4 T cells in lymph nodes before SIV infection and at 4 or >12 w.p.i. for IFN-1ant (Ant, $n = 6$) and placebo (Plac, $n = 9$) macaques. Horizontal bars represent median values. *P* values at different time points within treatment groups were calculated by Wilcoxon matched pairs signed rank test and between groups by Mann–Whitney *U* test. **e**, Frequency of $CCR5^+$ memory ($CD28^+CD95^+$ or $CD28^-CD95^{+/-}$) CD4 T cells in peripheral blood in macaques treated with IFN-1ant ($n = 6$) or placebo saline ($n = 9$). Error bars indicate range. Red vertical line indicates day 0 of systemic SIV infection. Shading indicates treatment period. *P* values represent the comparison between groups of the AUC (0–12 w.p.i. and 4–12 w.p.i.). **f**, Frequency of $CCR5^+$ memory CD4 T cells in lymph nodes in macaques treated with IFN-1ant ($n = 6$) or placebo saline ($n = 9$). Horizontal bars represent median values. *P* values at different time points within treatment groups were calculated by Wilcoxon matched pairs signed rank test and between groups by Mann–Whitney *U* test. **g**, Kaplan–Meier survival curve comparing macaques treated with IFN-1ant ($n = 6$) to macaques that received placebo ($n = 9$). *P* value indicates the significance by logrank (Mantel–Cox) test for survival by 32 w.p.i. For all panels, IFN-1ant-treated macaques are represented in red, placebo-treated macaques in blue.

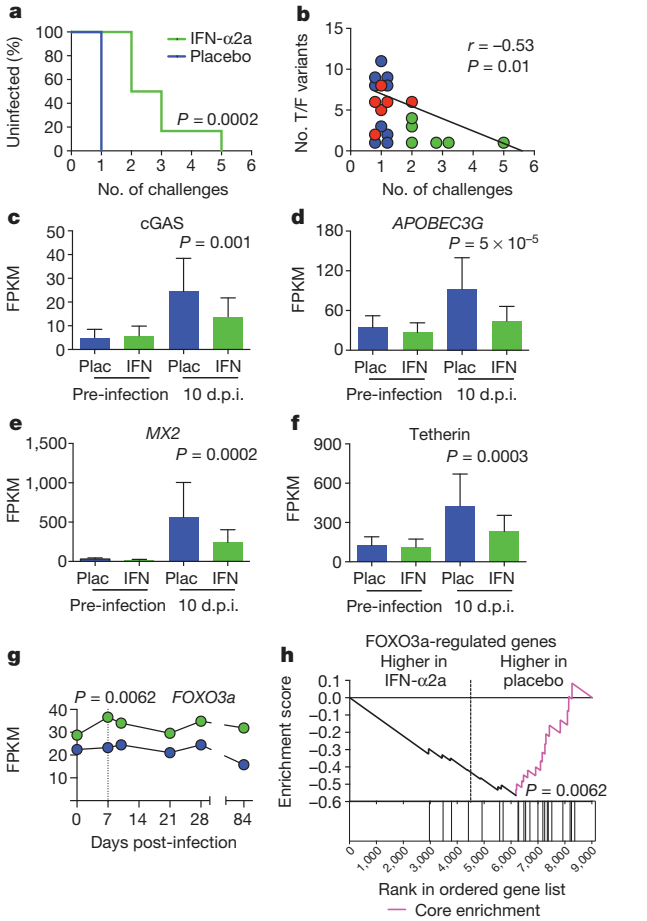

Figure 3 | IFN-α2a treatment transiently prevents systemic infection but results in an IFN-tolerant state. **a**, Kaplan–Meier survival curve comparing the number of SIV_{MAC251} rectal challenges required to achieve systemic infection in macaques treated with IFN-α2a ($n = 6$) or placebo saline ($n = 9$). *P* value indicates the significance by logrank (Mantel–Cox) test of the number of challenges required for systemic infection, between 1 and 5 challenges. **b**, Correlation between the number of challenges needed to achieve systemic infection and the number of transmitted/founder (T/F) variants in IFN-α2a (green, $n = 6$), IFN-1ant (red, $n = 6$) and placebo (blue, $n = 9$) macaques. *P* value indicates the significance of the correlation between the number of challenges and the number of T/F variants in all groups. *r* indicates the Spearman's rank correlation coefficient. **c–f**, Expression of antiviral mediators in PBMCs in IFN-α2a-treated (IFN, $n = 6$) macaques compared to placebo (Plac, $n = 9$) at 10 d.p.i. Error bars indicate range. *P* values represent the comparison of FPKMs between IFN-α2a and placebo at 10 d.p.i. by Mann–Whitney *U* test. **g**, Expression profile of *FOXO3a*, a negative regulator of type I IFN signalling. *P* value represents the comparison of *FOXO3a* FPKM between IFN-α2a ($n = 6$) and placebo ($n = 9$) macaques at 7 d.p.i. **h**, Gene-set enrichment analysis in IFN-α2a ($n = 6$) and placebo ($n = 9$) macaques of genes previously demonstrated to be overexpressed in $FOXO3^{-/-}$ macrophages[25]. The line plot indicates the running-sum of the enrichment score; the leading edge is indicated in magenta. The relative positions of all genes within the ranked data set are shown in the stick plot below the *x* axis. *P* value indicates statistical significance of the enrichment score, reflecting lower cumulative ranking of FOXO3a targets in IFN-α2a-treated macaques compared to placebo at 7 d.p.i. For all panels, IFN-α2a-treated macaques are represented in green, placebo-treated macaques in blue.

IFN-α2a treatment in the unchallenged macaques, increased *FOXO3a* expression was associated with ISG downregulation (Extended Data Fig. 6f). While these data do not exclude additional mechanisms, they suggest that ISG downregulation in the IFN-α2a-treated macaques was a consequence of endogenous homeostatic control rather than neutralization of exogenous IFN-α2a. Thus, exogenous augmentation of IFN-I signalling was associated with enhanced protection against SIV acquisition, but susceptibility to exacerbated systemic infection once ISG expression waned.

Given their roles in virus control, T and NK cells were evaluated. No changes in SIV-specific CD4 or CD8 T-cell responses developed with repeated challenges, suggesting that resistance to infection did not depend on adequate T-cell responses (Supplementary Information). However, higher circulating $CD56^+$ NK-cell frequencies after starting IFN-α2a predicted more challenges necessary for infection and were associated with resistance to infection (Extended Data Fig. 8c). Once the $CD56^+$ NK-cell

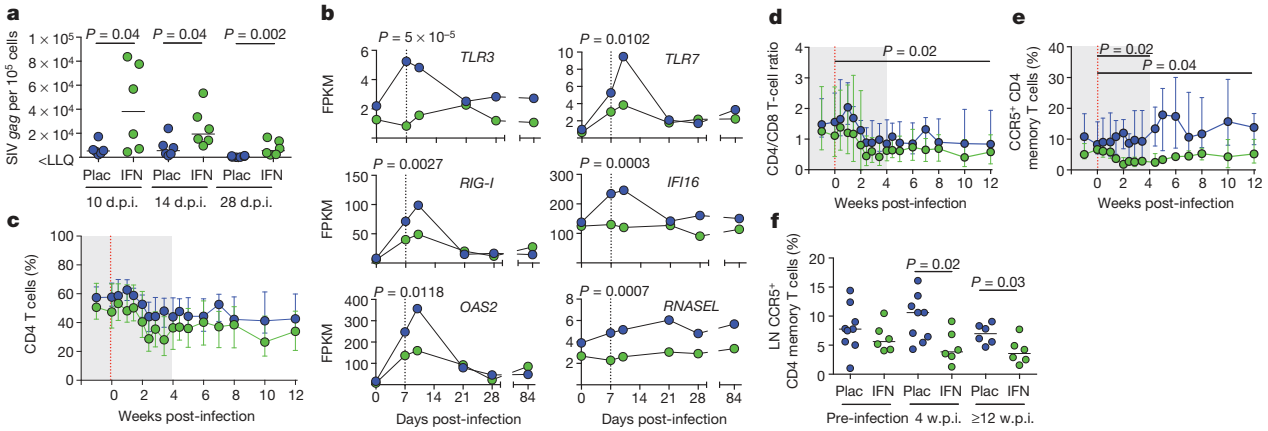

Figure 4 | IFN-α2a accelerates disease progression. **a**, PBMC-associated SIV *gag* DNA at 10, 14 and 28 d.p.i. in IFN-α2a macaques (IFN, $n = 6$) and placebo (Plac, $n = 6$) macaques. LLQ indicates lower limit of quantification. Horizontal bars represent median values. *P* values were calculated by Mann–Whitney *U* test. **b**, Expression of differentially expressed genes involved in pattern recognition receptor signalling. *P* values represent the comparison between FPKMs of IFN-α2a ($n = 6$) and placebo ($n = 9$) macaques at 7 d.p.i. **c**, Frequency of CD4 T cells in peripheral blood during acute and early SIV infection in IFN-α2a ($n = 6$) and placebo ($n = 9$) macaques. Error bars indicate range. Shading indicates treatment period. Red vertical line indicates day 0 of systemic SIV infection. **d**, CD4/CD8 T-cell ratio in peripheral blood during acute and early SIV infection in IFN-α2a ($n = 6$) and placebo ($n = 9$) macaques. Error bars indicate range. Shading indicates treatment period. Red vertical line indicates day 0 of systemic SIV infection. *P* value represents the comparison between groups of the AUC (0-12 w.p.i.). **e**, Frequency of $CCR5^+$ memory CD4 T cells in peripheral blood in IFN-α2a ($n = 6$) and placebo ($n = 9$) macaques. Error bars indicate range. Shading indicates treatment period. Red vertical line indicates day 0 of systemic SIV infection. *P* values represent the comparison between groups of the AUC (0-4 and 0-12 w.p.i.). **f**, Frequency of $CCR5^+$ memory CD4 T cells in lymph nodes in IFN-α2a ($n = 6$) and placebo ($n = 9$) macaques. Horizontal bars represent median values. *P* values were calculated by Mann–Whitney *U* test. For all panels, IFN-α2a-treated macaques are represented in green, placebo-treated macaques in blue.

frequency declined, the macaques became infected. In rectal biopsies at 28 d.p.i., more resistant macaques had higher $CD16^+$ NK-cell frequencies (Extended Data Fig. 8d). Together, these data suggest that IFN-α2a-induced innate immunity, rather than T-cell responses, protected against SIV infection.

Despite fewer transmitted/founder variants, pVLs did not differ significantly between IFN-α2a and placebo groups (Extended Data Fig. 8e), potentially obscured by the variability and small number of macaques. PBMC-associated SIV *gag* DNA levels, however, were significantly higher in the IFN-α2a group than placebo at 10, 14 and 28 d.p.i. (Fig. 4a). While the circulating CD4 T-cell frequency (Fig. 4c) and CD4/CD8 T-cell ratio (Fig. 4d) declined between 0 and 4 w.p.i. in both groups, the CD4/CD8 T-cell ratio was significantly lower in the IFN-α2a group (based on area under the curve (AUC) (0–12 w.p.i.)). The $CCR5^+$ memory CD4 T-cell frequency in blood was significantly lower in IFN-α2a than placebo macaques during acute (AUC(0–4 w.p.i.), Fig. 4e) and chronic infection (AUC(0–12 w.p.i.)) and in lymph nodes at 4 (Fig. 4f) and 12 w.p.i., although the frequency of CD4 T cells and CD4/CD8 T-cell ratio in lymph nodes and jejunum were similar between groups at 4 and ≥12 w.p.i. (data not shown). Thus, SIV-infected IFN-α2a-treated macaques had increased CD4 T-cell-associated virus load and greater CD4 T-cell loss with preferential depletion of the $CCR5^+$ subset.

We assessed whether increased immune activation was associated with this CD4 T-cell loss. The circulating $Ki67^+$ memory CD4 and CD8 T-cell frequencies were lower in the IFN-α2a compared to placebo group during acute infection only (AUC(0–4 w.p.i.)) with no differences in the frequencies of $HLA\text{-}DR^+$ memory T cells (Extended Data Fig. 9a–d). In the lymph nodes, the frequencies of $Ki67^+$ memory CD4 T cells at 4 w.p.i. and $HLA\text{-}DR^+$ memory CD4 T cells at ≥12 w.p.i. were significantly lower in the IFN-α2a than placebo group with no differences in CD8 T cells (Extended Data Fig. 9e–h). Thus, the IFN-α2a macaques had similar or less immune activation compared to placebo macaques.

We further explored the mechanisms underlying the increased cell-associated SIV and CD4 T-cell depletion in IFN-α2a macaques using whole-transcriptome sequencing of PBMCs. As with IFN-1ant, IFN-α2a administration significantly affected the PRR signalling pathway (Extended Data Fig. 10a). *C1q*, *TLR3*, *TLR7* and *RIG-I* were downregulated in the IFN-α2a macaques, yet expression of *IL-6*, *TNF* and *IL-1β* was increased at 7 d.p.i. (Fig. 4b and Extended Data Fig. 10b). Mediators of stress responses and cell survival downstream of IL-6 signalling, such as *MAP2K3*, and other anti-apoptotic genes such as *DIABLO* and *BCL2L1* were upregulated at 7 d.p.i. (Extended Data Fig. 10b, 10c), whereas pro-apoptotic genes including *CASP10* were downregulated. Thus, early IFN-α2a administration increased early expression of proinflammatory cytokines despite decreased PRR expression and delayed induction of apoptotic pathways.

We next assessed T- and NK-cell-mediated immunity. IFN-α2a-treated macaques had intact and even enhanced SIV-specific CD8 T-cell responses with no deficits in CD4 T-cell responses (Extended Data Fig. 8f–i and Supplementary Information). Whereas there were no differences at 4 w.p.i., between 4 and 12 w.p.i., the $CD56^+$ NK-cell frequency increased and $CD16^+$ NK-cell frequency decreased in the IFN-α2a but not the placebo group. The frequencies of $CD16^+$ (Extended Data Fig. 8j), $CD107a^+$ and granzyme B^+ NK cells at 12 w.p.i. were subsequently lower in the IFN-α2a-treated macaques compared to placebo.

Taken together, these data show that despite initially increasing ISG expression and conferring resistance to SIV infection, continued IFN-α2a treatment resulted in an IFN-desensitized state, with decreased antiviral gene expression, increased susceptibility to infection, increased cell-associated virus load and greater CD4 T-cell depletion compared to placebo.

Thus, both IFN-I receptor blockade and IFN-α2a administration ultimately resulted in decreased and delayed IFN-I responses, the biological outcomes of which reveal a pivotal role for IFN-I signalling in acute retroviral exposure in primates that overshadows the potential harm of increased inflammation. That a delay of as few as 3 days in antiviral gene expression resulted in accelerated disease progression suggests that SIV disease course is determined very early and depends upon the precise timing of peak antiviral activity. The observation of shortened time-to-death despite the eventual normalization of ISG expression during chronic infection clearly shows that a resurgence of late antiviral activity cannot compensate for compromised early virus control. Indeed, administration of IFN-α in chronic HIV infection has given inconsistent results for virus load and CD4 T-cell counts with no effect on disease outcome[7–9]. An interesting parallel to our study was recently described in mice with chronic lymphocytic choriomeningitis virus infection where persistent IFN-I signalling exerts antiviral effects but also leads to immune hyperactivation and suppression of antiviral

T-cell responses[14,15]. Our findings differ from a previous study that reported unchanged virus burden with IFN-α2a administration during chronic SIV infection[24] and a study of IFN-α2b or the IFN-αB/D chimaera in rhesus macaques challenged intravenously with highly pathogenic SIV $Delta_{B670}$ that showed no protection from infection but decreased peak antigenaemia[26]. The initial protection from infection and decrease in transmitted/founder variants observed in our study highlight the rectal mucosa's function as a barrier to SIV during transmission in the context of ISG induction. It is tempting to speculate that administration of IFN-α2a before SIV challenge also facilitated NK-cell activation and recruitment to the rectum and contributed to protection from infection[27]. Given the relative IFN-I resistance of transmitted/founder viruses[28,29] and the induction of an IFN-desensitized state associated with the upregulation of the IFN-I pathway repressor *FOXO3a* (ref. 25), our findings add a cautionary note to adjuvanted HIV vaccines or other prevention approaches that induce ISGs at mucosal surfaces. Furthermore, while the rectum contains many resident target CD4 T cells[30] that antiviral mediators can protect, sites with few resident target cells, such as the female genital tract[16], may depend on IFN-I signalling for CD4 T-cell recruitment and virus propagation. Thus, inflammation might attenuate transmission at the former site but exacerbate it at the latter[3]. In conclusion, disease progression in HIV infection emerges from the balance between the beneficial antiviral effects of inflammation, its detrimental systemic and immunologic effects, and its unique role of providing activated CD4 T-cell targets for HIV. Interfering with one part of this unstable equilibrium has unpredictable consequences. Thus, while there is good reason to use both pro- and anti-inflammatory therapeutic approaches in the treatment and prevention of HIV infection, they should be embarked upon with careful assessment of the virological and immunological consequences before widespread implementation.

Online Content Methods, along with any additional Extended Data display items and Source Data, are available in the online version of the paper; references unique to these sections appear only in the online paper.

Received 11 April; accepted 4 June 2014.
Published online 9 July 2014.

1. Hunt, P. W. *et al.* Gut epithelial barrier dysfunction and innate immune activation predict mortality in treated HIV infection. *J. Infect. Dis.* http://dx.doi.org/10.1093/infdis/jiu238 (21 April 2014).
2. Roberts, L. *et al.* Genital tract inflammation during early HIV-1 infection predicts higher plasma viral load set point in women. *J. Infect. Dis.* **205,** 194–203 (2012).
3. Naranbhai, V. *et al.* Innate immune activation enhances HIV acquisition in women, diminishing the effectiveness of tenofovir microbicide gel. *J. Infect. Dis.* **206,** 993–1001 (2012).
4. Schoggins, J. W. *et al.* A diverse range of gene products are effectors of the type I interferon antiviral response. *Nature* **472,** 481–485 (2011).
5. Schoggins, J. W. *et al.* Pan-viral specificity of IFN-induced genes reveals new roles for cGAS in innate immunity. *Nature* **505,** 691–695 (2013).
6. Gonzalez-Navajas, J. M., Lee, J., David, M. & Raz, E. Immunomodulatory functions of type I interferons. *Nature Rev. Immunol.* **12,** 125–135 (2012).
7. Lane, H. C. *et al.* Anti-retroviral effects of interferon-α in AIDS-associated Kaposi's sarcoma. *Lancet* **332,** 1218–1222 (1988).
8. Manion, M. *et al.* Interferon-alpha administration enhances CD8+ T cell activation in HIV infection. *PLoS ONE* **7,** e30306 (2012).
9. Azzoni, L. *et al.* Pegylated Interferon alfa-2a monotherapy results in suppression of HIV type 1 replication and decreased cell-associated HIV DNA integration. *J. Infect. Dis.* **207,** 213–222 (2013).
10. Feld, J. J. & Hoofnagle, J. H. Mechanism of action of interferon and ribavirin in treatment of hepatitis C. *Nature* **436,** 967–972 (2005).
11. Stacey, A. R. *et al.* Induction of a striking systemic cytokine cascade prior to peak viremia in acute human immunodeficiency virus type 1 infection, in contrast to more modest and delayed responses in acute hepatitis B and C virus infections. *J. Virol.* **83,** 3719–3733 (2009).
12. Fraietta, J. A. *et al.* Type I interferon upregulates Bak and contributes to T cell loss during human immunodeficiency virus (HIV) infection. *PLoS Pathog.* **9,** e1003658 (2013).
13. Abel, K. *et al.* The relationship between simian immunodeficiency virus RNA levels and the mRNA levels of α/β interferons (IFN-alpha/beta) and IFN-α/β-inducible Mx in lymphoid tissues of rhesus macaques during acute and chronic infection. *J. Virol.* **76,** 8433–8445 (2002).
14. Teijaro, J. R. *et al.* Persistent LCMV infection is controlled by blockade of type I interferon signaling. *Science* **340,** 207–211 (2013).
15. Wilson, E. B. *et al.* Blockade of chronic type I interferon signaling to control persistent LCMV infection. *Science* **340,** 202–207 (2013).
16. Li, Q. *et al.* Glycerol monolaurate prevents mucosal SIV transmission. *Nature* **458,** 1034–1038 (2009).
17. Haas, D. W. *et al.* A randomized trial of interferon alpha therapy for HIV type 1 infection. *AIDS Res. Hum. Retroviruses* **16,** 183–190 (2000).
18. Fernandez, S. *et al.* $CD4^+$ T-cell deficiency in HIV patients responding to antiretroviral therapy is associated with increased expression of interferon-stimulated genes in $CD4^+$ T cells. *J. Infect. Dis.* **204,** 1927–1935 (2011).
19. Levin, D. *et al.* Multifaceted activities of type I interferon are revealed by a receptor antagonist. *Sci. Signal.* **7,** ra50 (2014).
20. Goujon, C. *et al.* Human MX2 is an interferon-induced post-entry inhibitor of HIV-1 infection. *Nature* **502,** 559–562 (2013).
21. Honda, K. *et al.* IRF-7 is the master regulator of type-I interferon-dependent immune responses. *Nature* **434,** 772–777 (2005).
22. Barouch, D. H. *et al.* Vaccine protection against acquisition of neutralization-resistant SIV challenges in rhesus monkeys. *Nature* **482,** 89–93 (2012).
23. Carrington, M. & Alter, G. Innate immune control of HIV. *Cold Spring Harb. Perspect. Med.* **2,** a007070 (2012).
24. Asmuth, D. M. *et al.* Pegylated interferon-α 2a treatment of chronic SIV-infected macaques. *J. Med. Primatol.* **37,** 26–30 (2008).
25. Litvak, V. *et al.* A FOXO3–IRF7 gene regulatory circuit limits inflammatory sequelae of antiviral responses. *Nature* **490,** 421–425 (2012).
26. Schellekens, H. *et al.* The effect of recombinant human interferon αB/D compared to interferon α2b on SIV infection in rhesus macaques. *Antiviral Res.* **32,** 1–8 (1996).
27. Waggoner, S. N., Daniels, K. A. & Welsh, R. M. Therapeutic depletion of natural killer cells controls persistent infection. *J. Virol.* **88,** 1953–1960 (2014).
28. Parrish, N. F. *et al.* Phenotypic properties of transmitted founder HIV-1. *Proc. Natl Acad. Sci. USA* **110,** 6626–6633 (2013).
29. Fenton-May, A. E. *et al.* Relative resistance of HIV-1 founder viruses to control by interferon-alpha. *Retrovirology* **10,** 146 (2013).
30. McElrath, M. J. *et al.* Comprehensive assessment of HIV target cells in the distal human gut suggests increasing HIV susceptibility toward the anus. *J. Acquir. Immune Defic. Syndr.* **63,** 263–271 (2013).

Supplementary Information is available in the online version of the paper.

Acknowledgements We would like to acknowledge A. Zimin for his work in creating the MuSuRCA rhesus assembly, C. Miller for the gift of 6 rhesus macaques and Y. Peleg and S. Albeck at the Israel Structure Proteomic Center and G. Jona from Weizmann Institute Biological services for helping with protein production and purification; A. Roque and N. Haining for initial work on the pilot study; N. Modi, D. Ambrozak, R. Koup, M. Ghosh, I. Srivastava, R. Schwartz, F. Villinger, K. Zoon, J. Bekisz, K. Ghneim, A. Filali, R. Sekaly, L. Mach and L. Shen for their assistance on the current project; and A. Somasunderam for additional support. This project was supported by NIH Intramural Funding, federal funds from NCI/NIH Contract HHSN261200800001E, NIH R24 RR017444, NIH AI-076174, I-CORE Program of the Planning and Budgeting Committee and the Israel Science Foundation grant No. 1775/12.

Author Contributions N.G.S. designed and coordinated the study, developed and performed experiments, interpreted the data and prepared the manuscript. S.E.B. analysed and interpreted the sequencing data, generated figures and contributed to manuscript preparation. J.D.E. contributed to study design and developed and performed *in situ* hybridization and immunohistochemistry assays. R.T.R.Z. processed samples, performed flow cytometry and analysis, performed qRT–PCR and generated the sequencing libraries. G.K.T. analysed and interpreted the sequencing data and generated figures. E.B. developed the library generation protocol and supervised library generation. D.L. and G.Y. synthesized the IFN-1ant. S.W. generated sequencing libraries and assisted in analysis of the sequencing data. K.N.M. assisted with sample processing, performed flow cytometry assays, and assessed plasma for neutralizing activity. G.Q.d.P. evaluated circulating SIV for IFN resistance. B.J.H. designed, performed and analysed qRT–PCR assays. J.K.T. processed samples and performed ELISAs. E.R. assisted with sample processing and performed flow cytometry assays. S.D. assisted with sequencing analysis. E.C. assisted with sample processing and performed flow cytometry assays. J.P.T. performed SIV inoculations and coordinated the study at Bioqual. G.Si. established the Non-Human Primate Sequencing Core and facilitated sequencing analysis and contributed to data interpretation. M.N. assisted with statistical analyses. R.B.N. generated the MuSuRCA *Macaca mulatta* assembly. B.F.K. sequenced the transmitted/founder variants. S.R. contributed to study design and followed the rhesus macaques clinically. J.A.L. contributed to IFN-1ant design and assisted with analysis. J.D.L. contributed to study design, assessment for IFN-resistant viruses and manuscript preparation. G.Sc. contributed to study design, IFN-1ant design and production and assisted with analysis. D.C.D. designed and supervised the study, interpreted the data and prepared the manuscript.

Author Information Gene expression data are available at the Gene Expression Omnibus under accession codes GSM1298835 through GSM1299037. Reprints and permissions information is available at www.nature.com/reprints. The authors declare competing financial interests: details are available in the online version of the paper. Readers are welcome to comment on the online version of the paper. Correspondence and requests for materials should be addressed to D.C.D. (ddouek@mail.nih.gov).

METHODS

Dose escalation study. We performed a dose escalation study in two rhesus macaques with chronic SIV_{MAC251} infection and different frequencies of CD4 T cells and $CCR5^+$ CD4 and CD8 T cells to maximize the likelihood of detecting a response. IFN-1ant was dosed three times a week based on dosing of recombinant IFN-α2a (Roferon-A, Roche, Switzerland) for hepatitis C infection. We administered 50 μg of IFN-1ant for one week, 200 μg for one week, 500 μg for one week and 800 μg for one week. Based on a dose-dependent increase in CD4 T-cell frequency and decrease in the frequencies of $CCR5^+$ CD4 and $CCR5^+$ and $Ki67^+$ CD8 T cells (Extended Data Fig. 1a–d), and because of ease of administration, we decided on 1 mg of IFN-1ant. Daily dosing was chosen as the effects appeared to be variable based on the time since last dosing.

Macaques and experimental design. To examine the effects of blocking type I IFN signalling, healthy, SIV-uninfected Mamu $A01^-B08^-B17^-$ adult *Macaca mulatta* received 1 mg daily intramuscularly of the IFN-I receptor antagonist (IFN-1ant, 1 mg ml^{-1}, $n = 6$; synthesized as previously described[19]) or 1 ml normal saline ($n = 9$) by intramuscular injection for 4 weeks (see Extended Data Fig. 1e). The macaques were inoculated weekly, starting the first day of treatment, with 1 ml of SIV_{MAC251} via rectal challenge (1 ml of a 1:25 dilution, stock 3×10^8 SIV RNA copies ml^{-1}), up to three times until infection was confirmed (SIV pVL >250 copies ml^{-1}). Blood was sampled several times per week, and lymph node and jejunal biopsies were performed before treatment and at the end of the 4-week period. All blood draws and biopsies were performed before inoculation with SIV_{MAC251} and before any drug administration on that day. The macaques were followed for up to 40 w.p.i.

To examine the effect of exogenous IFN-I treatment, six healthy, SIV-uninfected Mamu $A01^-B08^-B17^-$ adult macaques received 6 μg kg^{-1} pegylated IFN-α2a (Pegasys, Genentech USA) intramuscularly weekly starting one week before the first SIV_{MAC251} inoculation. Dose was based on prior efficacy studies in rhesus macaques[24]. The macaques were challenged intrarectally weekly on the same day as, but before, IFN-α2a administration, with the same high-dose SIV_{MAC251} inoculation as the IFN-1ant and placebo macaques, until infection was confirmed. All blood draws and biopsies were performed before inoculation with SIV_{MAC251} and before any drug administration on that day. The macaques were followed for a total of 12 weeks after infection and then euthanized per protocol. To examine the effect of exogenous IFN-I treatment in the absence of SIV infection, three healthy, SIV-uninfected Mamu $A01^-B08^-B17^-$ adult macaques received 6 mg kg^{-1} pegylated IFN-α2a (Pegasys, Genentech USA) intramuscularly weekly for 3 weeks. Blood was sampled twice weekly starting 1 week before IFN-α2a treatment through to 1 week after the last dose. The lymph node, jejunum and rectum were biopsied before IFN-α2a treatment, 1 week after the first dose and 1 week after the last dose.

All macaques were housed at Bioqual, Inc., and assigned randomly to treatment or placebo arms. TRIMCyp, the fusion protein derived from TRIM5 and cyclophilin A, was present in 1 placebo macaque, 2 IFN-1ant macaques and 0 IFN-α2a macaques. One TRIM5α SPRY deletion was present in 4 placebo macaques, 3 IFN-1ant macaques and 1 IFN-α2a macaque (the macaque that required 5 challenges to become systemically infected) and two TRIM5α SPRY deletions in 2 IFN-1ant macaques. There was no significant difference in genotype distribution between placebo and IFN-1ant macaques or between placebo and IFN-α2a macaques based on Fisher's test. Based on availability, the 6 IFN-1ant macaques and 9 placebo macaques were male and ages 4 to 7 years, and the 6 IFN-α2a macaques were female with ages 9 to 15 years. The Vaccine Research Center Animal Care and Use Committee approved all study protocols and procedures.

Samples. Blood was collected in EDTA tubes. Plasma was collected and PBMCs were isolated by Ficoll density centrifugation. All of the jejunum and half the lymph node biopsy tissues and half of every tissue collected at necropsy were placed in RPMI with 10% fetal bovine serum (FBS) and transported on wet ice. The remaining tissues were placed in 4% paraformaldehyde and kept at room temperature overnight before being transferred to 80% ethanol and stored at 4 °C. Tissues were subsequently paraffin-embedded for *in situ* hybridization and immunohistochemistry. Intestinal samples were incubated with RPMI + collagenase D (1 mg ml^{-1}) (Roche) + Penicillin-Streptomycin-Glutamine (Gibco) at 37 °C for 30 min and then passed through a 70 μm filter. Lymph node samples were passed through a 70 μm filter to remove debris. Cells isolated from both peripheral blood and tissues were either stained for flow cytometry or cryopreserved.

Flow cytometry. Cellular activation and cell cycle entry were assessed by flow cytometry. PBMCs and cells from the jejunum and lymph nodes were stained with Aqua LIVE/DEAD Fixable Dead Cell Stain and antibodies to the following: CD4 Qd605, CD8 Qd655 (Invitrogen); CD3 APC-Cy7, CD95 PE-Cy5, CD14 Pacific Blue, CCR5 PE, CCR7 PE-Cy7, Ki67 FITC (BD Biosciences); CD28 ECD (Beckman Coulter); and HLA-DR Alexa 700PE (BD Biosciences, in-house conjugate). Cells were permeabilized using a Cytofix/Cytoperm kit (BD Biosciences) for Ki67 detection and fixed with 1% formaldehyde (Tousimis).

To assess antigen-specific responses and NK cell subsets, cryopreserved PBMCs were stimulated for 6 h at 37 °C with SIV Gag/Env/Pol peptide pool (2 μg ml^{-1}) in the presence of CD28 and CD49d (BD Biosciences) and brefeldin A (Sigma, 10 μg ml^{-1}). Cells were stained with Aqua LIVE/DEAD Fixable Dead Cell Stain (Invitrogen) and antibodies to the following: CD3 APC-Cy7, CD14 Pacific Blue, IFN-γ Cy7PE, TNF APC, CD107a FITC (BD Biosciences); Granzyme B PE (Caltag); CD4 Qd605, CD8 Qd655 (Invitrogen); CD16 Ax594, CD20 Ax700PE, CD56 Cy5PE, Perforin Ax680 (in-house conjugates, BD Biosciences). Cells were permeabilized using a Cytofix/Cytoperm kit (BD Biosciences) for intracellular cytokine detection and fixed with 1% formaldehyde (Tousimis).

To evaluate cellular exhaustion, cryopreserved PBMCs were stimulated for 6 h at 37 °C with SIV Gag/Env/Pol peptide pool (2 μg ml^{-1}) in the presence of brefeldin A (10 μg ml^{-1}). Cells were stained with Aqua LIVE/DEAD Fixable Dead Cell Stain (Invitrogen) and antibodies to the following: CD3 APC-Cy7, CD95 Cy5PE, IFN-γ FITC, TNF APC, Bcl-2 PE (BD Biosciences); CD28 ECD (Beckman Coulter); ICOS Pacific Blue (Biolegend); CD4 Qd605, CD8 Qd655, Streptavidin Cy7PE (Invitrogen); PD-1 biotinylated (R&D Systems). Cells were permeabilized using a Cytofix/Cytoperm kit (BD Biosciences) for intracellular cytokine detection and fixed with 1% formaldehyde (Tousimis).

Transmitted/founder variant characterization. The number of transmitted/founder variants were characterized blindly, as previously described[28], and deposited in GenBank under accession numbers KJ201031 to KJ201503.

Determination of susceptibility of circulating SIV to IFN-α. Freshly isolated, CD8-depleted PBMCs from naive rhesus macaque donors were stimulated for 3 days with 5 μg ml^{-1} PHA and 100 U ml^{-1} IL-2 in RPMI supplemented with 10% FBS, 2 mM L-glutamine, 100 U ml^{-1} penicillin and 100 μg ml^{-1} streptomycin (RPMI-Complete). Target cells were re-suspended at 10^6 cells ml^{-1} in RPMI-Complete containing various concentrations of recombinant human IFN-α (PBL Interferon Source) and incubated at 37 °C for 4 h. IFN-α-containing culture supernatants were collected and stored at 37 °C. Target cells were split into duplicate cultures and spinoculated for 2 h at 800*g* with diluted, equivalent input amounts of SIV from plasma from 14 to 18 d.p.i. from IFN-α2a or placebo macaques. Cells were washed and re-suspended in matched, stored IFN-α containing supernatants supplemented with 100 U ml^{-1} IL-2. After incubation at 37 °C for 7 days, cell-free culture supernatants were collected and a SIV p27 antigen capture assay was used to detect the presence of viral p27 antigen according to the manufacturer's instructions (ABL).

Binding and neutralizing antibody assays. IFN-binding antibodies were assessed as previously described[31]. To evaluate for neutralizing antibodies, A549 cells (American Type Culture Collection, Manassas, VA) were seeded at 1×10^4 per well in RPMI with 2% FBS and 2 mM L-glutamine and incubated for 24 h. For the standard curve, IFN-α2b (Hoffman La Roche, Nutley, NJ) was added to cells in twofold serial dilution from 5 IU ml^{-1} to 0.04 IU ml^{-1}. For measurement of IFN-α2b-neutralizing antibodies in plasma, IFN-α2b was added at a concentration of 0.5 IU ml^{-1} along with 160-fold diluted plasma. Control wells received medium only or 5 IU ml^{-1} IFN-α2b and 13.1 μg ml^{-1} of a control neutralizing antibody. After an additional 24 h, the media was removed and replaced with RPMI 1640 containing 2% FBS, 2 mM L-glutamine containing encephalomyocarditis virus (EMCV, American Type Culture Collection, Manassas, VA) at a multiplicity of infection of 0.5. Cells were stained with crystal violet at 52 h and assessed for cytopathic effect as measured by optical density at 570 nm.

Quantitative RT–PCR. RNA was extracted from PBMCs preserved in TRIzol (Life Technologies) or from thawed cryopreserved PBMCs by RNAzol RT (Molecular Research Center, Inc.) according to the manufacturers' instructions. Purified RNA was added directly to a one-step quantitative RT–PCR reaction containing iScript RT-iTaq Taq enzyme mix (BioRad). MX1, OAS2 and β2 microglobulin were labelled with a 5′ FAM reporter and 3′ BHQ1 quencher (Biosearch Technologies). We used the following oligonucleotide sequences: *MX1* F AGGAGTTGCCCTTCCCAGA, *MX1* R CCTCTGAAGCATCCGAAATC, *MX1* P TGACCAGATGCCCGCTGGTG; *OAS2* F CAGTCCTGGTGAGTTTGCAGT, *OAS2* R CAGCGAGGGTAAATCCTTGA, *OAS2* P GCACTGGCATCAACAGTGCCAGA.

MX1 and *OAS2* forward and reverse primers were used at 500 nM, and probes at 200 nM. Samples were run on an Applied Biosystems Sequence Detection System 7900HT (ABI). Expression levels of *MX1* and *OAS2* were normalized to β2 microglobulin and calculated based on the ΔΔCT method.

Transcriptome analysis. Total RNA was prepared as described above. Polyadenylated transcripts were purified on oligo-dT magnetic beads, fragmented, reverse transcribed using random hexamers and incorporated into barcoded cDNA libraries based on the Illumina TruSeq platform. Libraries were validated by microelectrophoresis, quantified, pooled and clustered on Illumina TruSeq v2 flowcells. Clustered flowcells were sequenced on an Illumina HiSeq 2000 in 100-base single-read reactions.

New rhesus macaque genome. RNA-Seq data were analysed by alignment to a provisional assembly (deposited under BioProject accession PRJNA214746) and annotation of a new Indian *Macaca mulatta* genome (data provided by R.B.N., University of Nebraska Medical Center and A. Zimin, University of Maryland). Comparison of

RNA-seq data generated using the v.4 assembly demonstrated a greater absolute number of mapping reads, higher proportion of mapped reads per sample than to the hg19 RefSeq or RheMac2 assembly (Supplementary Fig. 1 and Supplementary Information).

RNA-seq data analysis. RNA-seq data were submitted to The Gene Expression Omnibus (GEO) repository at the National Center for Biotechnology Information (NCBI). RNA-seq data were aligned to a provisional assembly of Indian *Macaca mulatta* (MuSuRCA rhesus assembly v.4) using STAR version 2.3.0e[32]; parameters were set using the annotation as a splice junction reference, un-annotated non-canonical splice junction mappings and non-unique mappings were removed from downstream analysis. Transcripts were annotated using the provisional UNMC annotation v4.12. Transcript assembly, abundance estimates and differential expression analysis were performed using Cufflinks v2.1.1 and Cuffdiff[33]. Samples with <49% mapped reads or exhibiting considerable 3′ or 5′ bias were excluded from further analysis. To reduce normalization bias due to varying read depths, samples were analysed in two separate groups: group 1 comprised 166 samples and contained the samples from PBMCs from the placebo+SIV, IFN-1ant+SIV, and pegylated IFN-α2a-treated+SIV animals, and from samples for the analysis of PBMCs, LN CD4 T cells and rectal biopsies of uninfected, IFN-α2a-treated animals; the average number of mapped reads was 12,188,890 (range: 3,237,374–87,371,564). Group 2 comprised the lymph node CD4 T cells from the three SIV-infected groups consisting of 37 samples; the average mapped read count for this group was 4,898,448 (range: 1,173,455–19,310,483). Differentially expressed genes were defined by pair-wise comparison of each time point to the Day 0 baseline. We included genes that had any acute time point (0 vs 7, 10, 21, 28) that was significantly differentially expressed by a fixed discovery rate-corrected *P* value (q value) < 0.05. Differential gene lists were uploaded to Ingenuity Pathway Analysis software (v1.0 Ingenuity Systems, http://www.ingenuity.com/) and pathways with significant enrichment by Fisher's exact test and the Benjamini–Hochberg multiple testing correction were identified. Heat maps and other visualization were generated using Partek Genomics Suite v6.6.

Gene-set enrichment analysis (GSEA). GSEA was performed using the desktop module available from the Broad Institute (http://www.broadinstitute.org/gsea/). FPKMs for samples from the IFN-α2a and placebo groups at 7 d.p.i. were pre-filtered to remove transcripts with insufficient read coverage, and then were ranked using the signal-to-noise statistic. The gene-set was comprised of genes determined to be upregulated in unstimulated *FOXO3*$^{-/-}$ macrophages relative to macrophages from control mice[25]. Significance was estimated using gene-set permutation.

SIV *in situ* hybridization, immunohistochemistry and quantitative image analysis. SIV *in situ* hybridization was performed as previously described[34]. Immunohistochemistry for rabbit polyclonal anti-APOBEC3G (Prestige Antibodies Powered by Atlas Antibodies HPA001812; Sigma-Aldrich), TRIM5α (Prestige Antibodies Powered by Atlas Antibodies HPA023422; Sigma-Aldrich) and MX2 (Prestige Antibodies Powered by Atlas Antibodies HPA030235; Sigma-Aldrich) were performed using a biotin-free polymer approach (Rabbit Polink-2, Golden Bridge International, Inc.) on 5 μm tissue sections mounted on glass slides, which were dewaxed and rehydrated with double-distilled H_2O. Antigen retrieval was performed by heating sections in 0.01% citraconic anhydride containing 0.05% Tween-20 in a pressure cooker set at 122 °C for 30 s. Slides were rinsed in ddH_2O, incubated with blocking buffer (TBS containing 0.25% casein) and incubated with diluted rabbit anti-APOBEC3G, rabbit anti-TRIM5α or rabbit anti-MX2 in blocking buffer overnight at 4 °C. Tissue sections were rinsed in wash buffer (1 × TBS containing 0.05% Tween-20) for 10 min followed by an endogenous peroxidase blocking step using 1.5% (v/v) H_2O_2 in TBS (pH 7.4) for 10 min and placed in wash buffer. Slides were incubated with rabbit Polink-2 HRP polymer-staining system (Golden Bridge International, Inc.) according to manufacturer's recommendations (20–30 min at room temperature) then rinsed in wash buffer. Tissue sections were developed with Impact 3,3′-diaminobenzidine (Vector Laboratories), counterstained with haematoxylin and mounted in Permount (Fisher Scientific). All stained slides were scanned at high magnification (× 200) using the ScanScope CS System (Aperio Technologies, Inc.) yielding high-resolution digital scans of the entire tissue section. Regions of interest of defined area (ROIs; 500 μm^2) were saved on the digital image using the Aperio rectangle tool (representing nearly the entire lymph node section) and high-resolution images were extracted from the ROIs of each whole-tissue scan. The per cent area of the lymph node (all anatomical compartments were included) that stained for APOBEC3G, TRIM5α and MX2 were quantified under blind analysis using Photoshop CS5 and Fovea tools.

Statistical methods. Based on our previous data of rhesus macaques with acute SIV infection, the standard deviation for SIV RNA levels is 0.5×10^6 copies ml^{-1}. Using this value, 6 macaques in the IFN-1ant or IFN-α2a group and 9 macaques in the placebo group would give us 80% power to detect a 0.8×10^6 copies ml^{-1} difference in SIV RNA levels between IFN-1ant or IFN-α2a and placebo groups. Macaques were assigned to their respective groups randomly. Experiments, except as noted above, were not performed blindly. All replicates are biological replicates. Each experiment was performed once. Comparisons between groups at singular time points were performed with the Mann–Whitney *U* test, comparisons within groups with the Wilcoxon matched-pairs signed rank test, survival curve comparisons for per cent survival (IFN-1ant) and per cent uninfected (IFN-α2a) with the log-rank (Mantel-Cox) test and correlations with Spearman coefficient, all using GraphPad Prism v5.0d. Comparisons of AUCs were performed using linear regression analysis adjusting for baseline values on JMP v10.

31. Vanderford, T. H. *et al.* Treatment of SIV-infected sooty mangabeys with a type-I IFN agonist results in decreased virus replication without inducing hyperimmune activation. *Blood* **119,** 5750–5757 (2012).
32. Dobin, A. *et al.* STAR: ultrafast universal RNA-seq aligner. *Bioinformatics* **29,** 15–21 (2013).
33. Trapnell, C. *et al.* Differential analysis of gene regulation at transcript resolution with RNA-seq. *Nature Biotechnol.* **31,** 46–53 (2013).
34. Brenchley, J. M. *et al.* Differential infection patterns of CD4+ T cells and lymphoid tissue viral burden distinguish progressive and nonprogressive lentiviral infections. *Blood* **120,** 4172–4181 (2012).

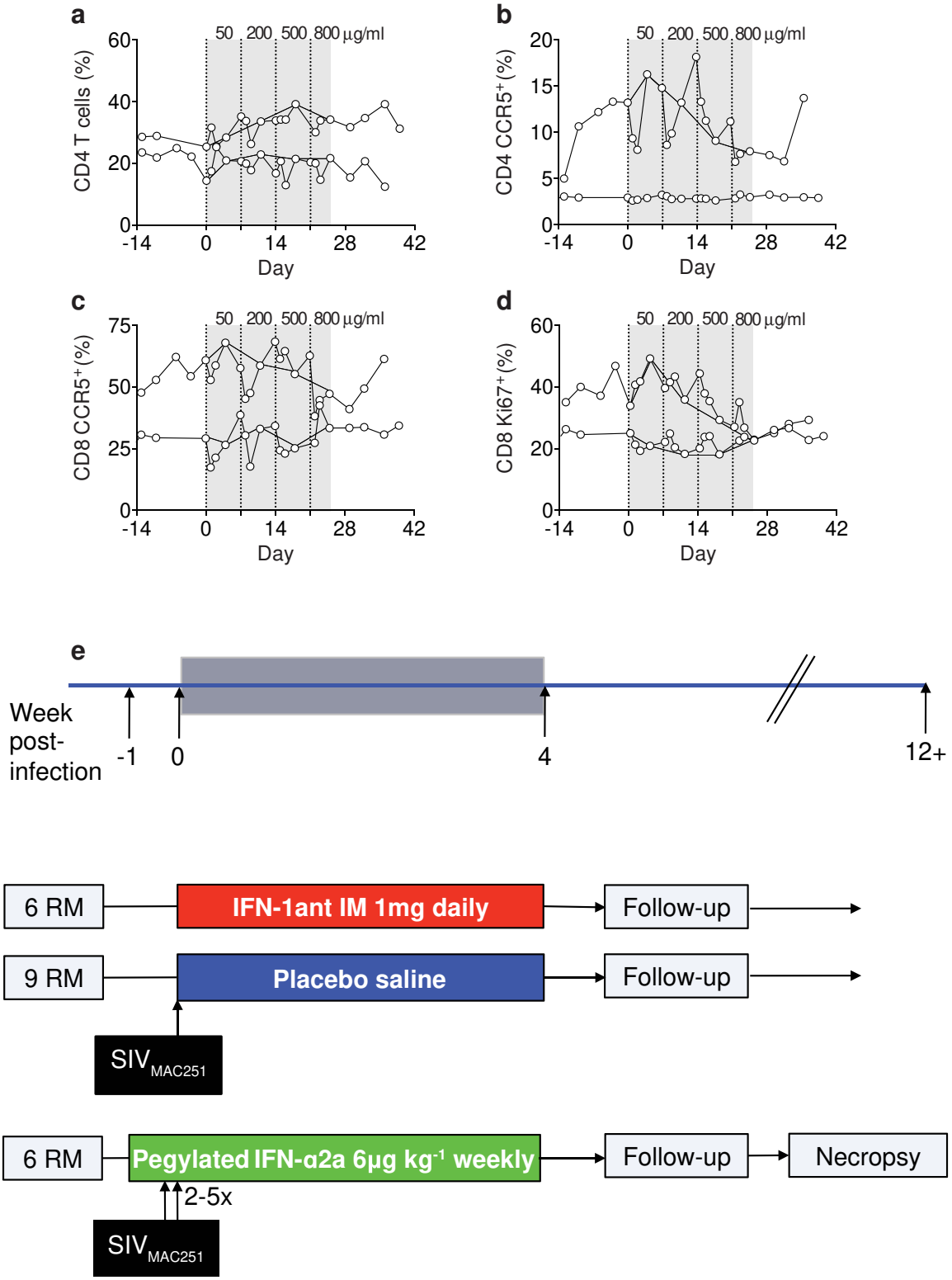

Extended Data Figure 1 | Dose escalation study for IFN-1ant and experimental schema. a–d, Effects of three times weekly IFN-1ant dosing on the frequency of CD4 T cells (**a**), CCR5$^+$ CD4 T cells (**b**), CCR5$^+$ CD8 T cells (**c**) and Ki67$^+$ CD8 T cells (**d**) in 2 rhesus macaques. Dose was 50 µg in week 1, 200 µg in week 2, 500 µg in week 3 and 800 µg in week 4. Vertical dotted lines indicate the days a new dose was started. Black lines connect time points 4 days after the first dose. Grey shading indicates treatment period. **e**, Six macaques received 4 weeks of IFN-1ant intramuscularly starting at day 0 and were challenged intrarectally with 1 ml of a 1:25 dilution of SIV_{MAC251} (stock concentration 3×10^8 SIV RNA copies ml^{-1}) at day 0 and followed until developing end-stage AIDS. Nine macaques were treated with 4 weeks of placebo saline intramuscularly starting at day 0 and challenged intrarectally with SIV_{MAC251} at day 0 and followed. Six macaques were injected weekly with IFN-α2a starting 1 week before the first challenge and through 4 w.p.i. Macaques required 2, 3 or 5 challenges to acquire systemic infection. Thus, macaques received 6, 7 or 9 doses of IFN-α2a. Macaques were necropsied at 12 w.p.i. per protocol.

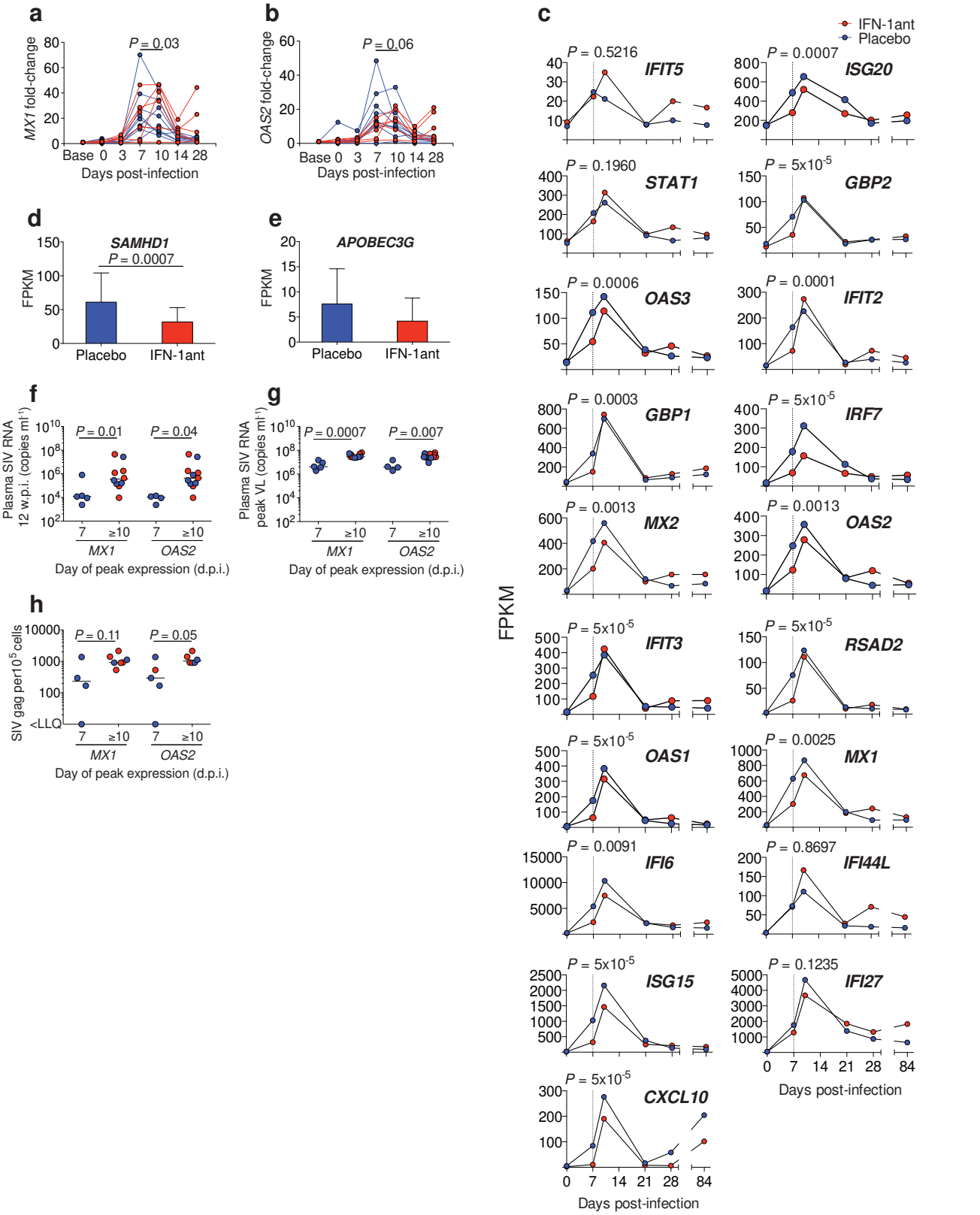

Extended Data Figure 2 | Effects of IFN-1ant on IFN-stimulated genes and virus burden. **a**, **b**, *MX1* (**a**) and *OAS2* (**b**) expression by qRT–PCR during acute SIV infection in IFN-1ant (red, $n = 6$) and placebo (blue, $n = 9$) macaques. *P* values were calculated by Mann–Whitney *U* test. **c**, ISGs in PBMCs in IFN-1ant and placebo macaques. *P* values represent the comparison between IFN-1ant ($n = 6$) and placebo ($n = 9$) macaque FPKMs at 7 d.p.i. **d**, **e**, *SAMHD1* (**d**) and *APOBEC3G* (**e**) expression in the lymph nodes in IFN-1ant ($n = 6$) and placebo ($n = 9$) macaques. *P* values were calculated by Mann–Whitney *U* test. **f**, **g**, Plasma SIV RNA levels at 12 w.p.i. (**f**) or at peak (**g**) stratified by the day that *MX1* or *OAS2* expression peaked in PBMCs in IFN-1ant ($n = 6$) and placebo ($n = 9$) macaques. VL, viral load. *P* values were calculated by Mann–Whitney *U* test. **h**, SIV *gag* levels in PBMCs stratified by the day that *MX1* or *OAS2* expression peaked in PBMCs in IFN-1ant ($n = 6$) and placebo ($n = 6$) macaques. *P* values were calculated by Mann–Whitney *U* test. For all panels, IFN-1ant-treated macaques are represented in red, placebo-treated macaques in blue.

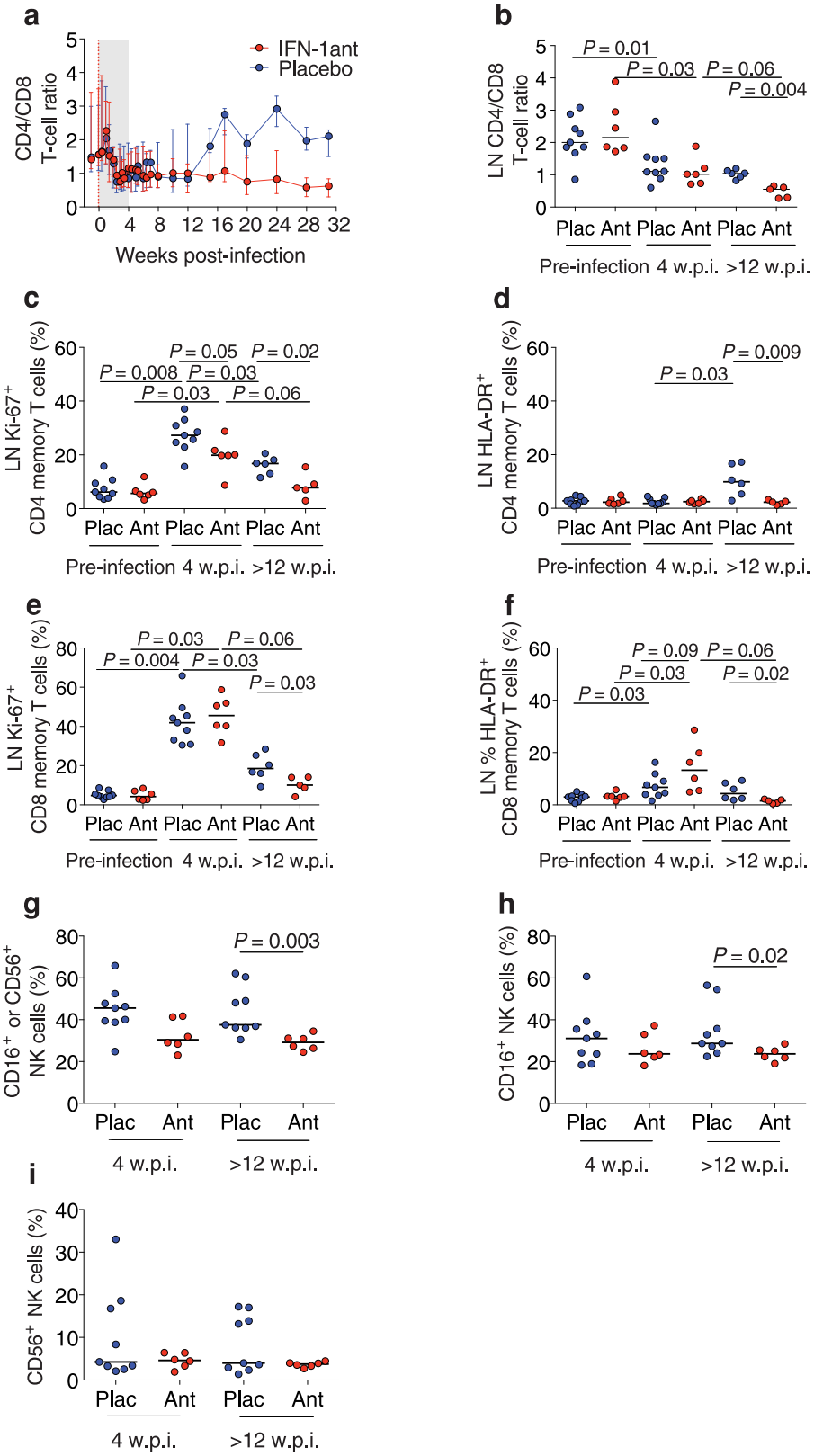

Extended Data Figure 3 | Effects of IFN-1ant on CD4 T cells and on immune activation. **a**, **b**, CD4/CD8 T-cell ratio in peripheral blood (**a**) and lymph node (LN) (**b**) in IFN-1ant (Ant, $n = 6$) and placebo (Plac, $n = 9$) macaques. Shading indicates treatment period. Error bars indicate range. Red vertical line indicates day 0 of systemic SIV infection. For all panels, horizontal bars indicate median values, and *P* values at different time points within treatment groups were calculated by Wilcoxon matched pairs signed rank test and between groups by Mann–Whitney *U* test. **c**–**f**, T-cell activation in lymph nodes (**c**–**f**) in CD4 (**c**, **d**) and CD8 (**e**, **f**) T cells as represented by the frequency of Ki67$^+$ (**c**, **e**) or HLA-DR$^+$ (**d**, **f**) cells in IFN-1ant ($n = 6$) and placebo ($n = 9$) macaques. **g**, Frequency of circulating CD16$^+$ or CD56$^+$CD3$^-$CD14$^-$ NK cells in IFN-1ant ($n = 6$) and placebo ($n = 9$) macaques. **h**, Frequency of circulating CD16$^+$ NK cells in IFN-1ant ($n = 6$) and placebo ($n = 9$) macaques. **i**, Frequency of circulating CD56$^+$ NK cells in IFN-1ant ($n = 6$) and placebo ($n = 9$) macaques. For all panels, IFN-1ant-treated macaques are represented in red, placebo-treated macaques in blue.

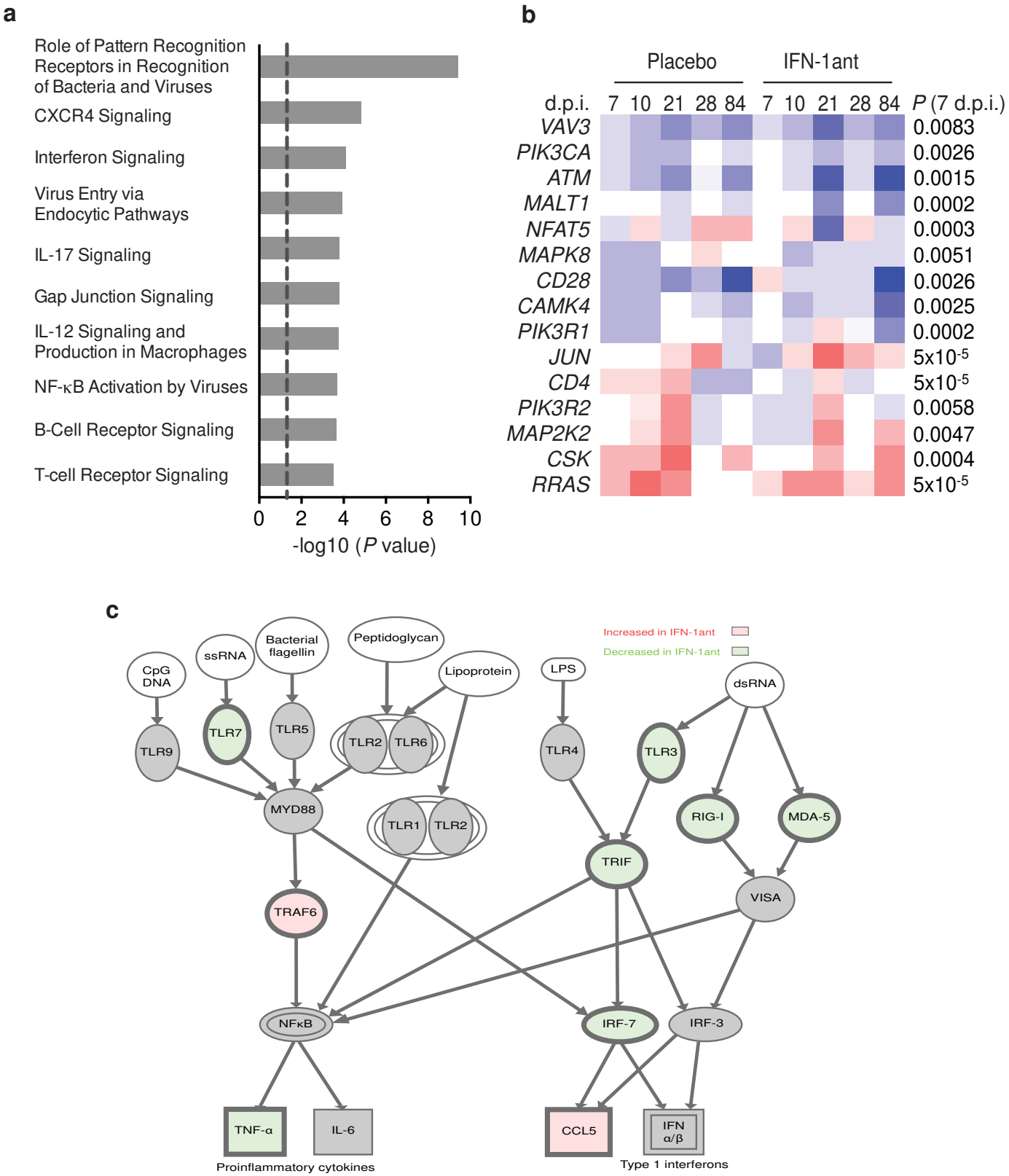

Extended Data Figure 4 | IFN-1ant alters innate and adaptive immune signalling. **a**, Selected pathways significantly affected by IFN-I blockade. *P* values were calculated by Fisher's exact test with the Benjamini–Hochberg multiple testing correction. **b**, Expression of genes involved in pattern recognition receptor signalling of IFN-1ant-treated macaques ($n = 6$) compared to placebo ($n = 9$) at 7 d.p.i. Upregulation compared to pre-infection is represented by red, no change by white, downregulation by blue. *P* values represent the comparison between IFN-1ant and placebo macaques at 7 d.p.i. **c**, Selected genes in pattern recognition receptor signalling pathways. Upregulation at 7 d.p.i. is represented by red, downregulation by green.

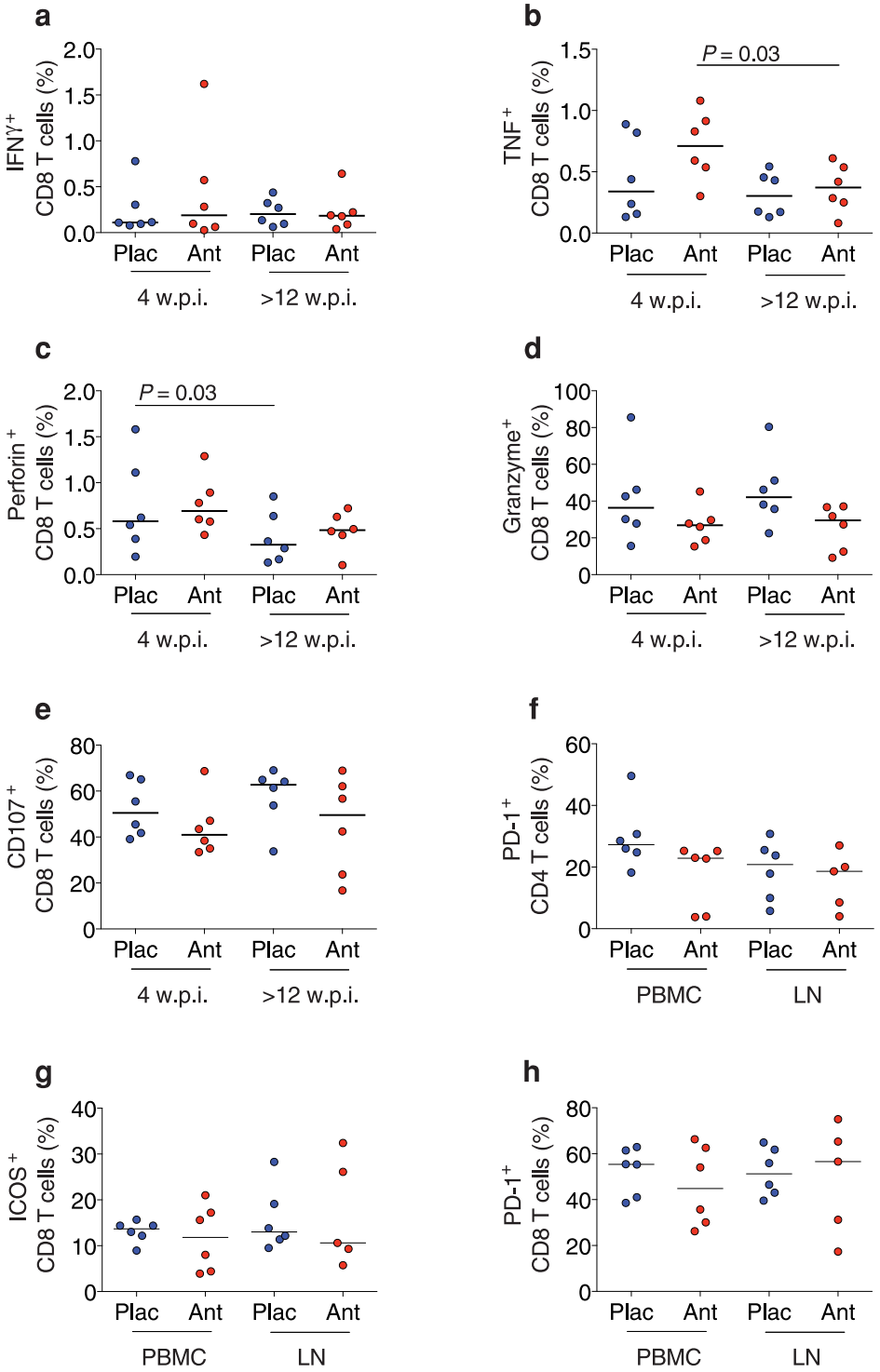

Extended Data Figure 5 | Effects of IFN-1ant on T-cell function and phenotype. a–e, SIV-specific responses in peripheral blood at 4 and >12 w.p.i. in IFN-1ant (Ant, $n = 6$) and placebo (Plac, $n = 6$) macaques by frequency of IFN-γ^+ (**a**), TNF$^+$ (**b**), perforin$^+$ (**c**), granzyme B$^+$ (**d**) and CD107$^+$ (**e**) CD8 T cells. T-cell exhaustion in peripheral blood and lymph nodes (LN) at >16 w.p.i. based on frequency of PD-1$^+$ CD4 (**f**) and CD8 (**h**) T cells and ICOS$^+$ (**g**) CD8 T cells. For all panels, *P* values at different time points within treatment groups were calculated by Wilcoxon matched pairs signed rank test and between groups by Mann–Whitney *U* test. IFN-1ant-treated macaques are represented in red, placebo-treated macaques in blue.

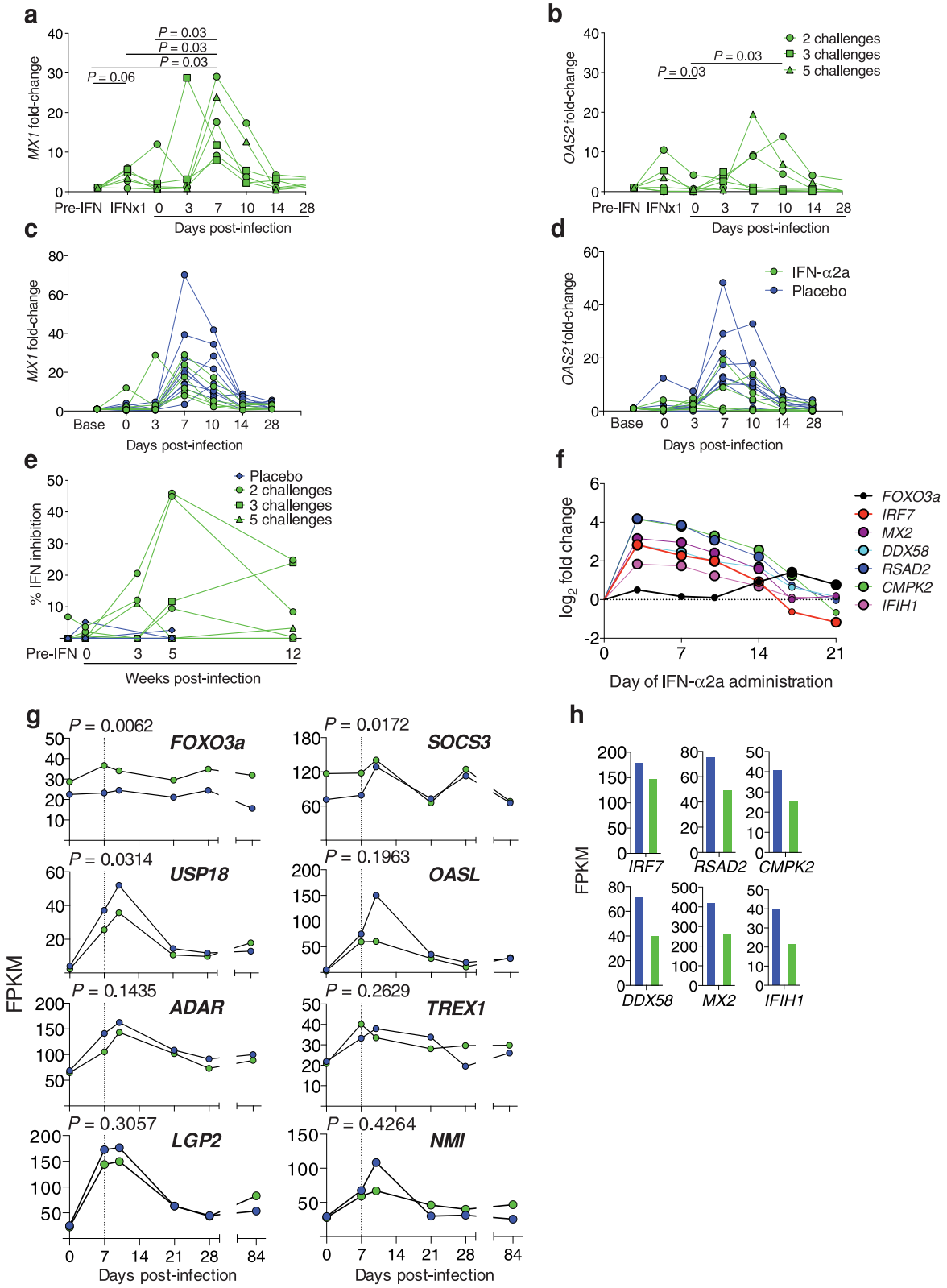

Extended Data Figure 6 | IFN-α2a treatment transiently induces ISGs and subsequently induces the IFN-repressor FOXO3a but does not induce neutralizing anti-IFN antibodies. a–d, *MX1* (**a**, **c**) and *OAS2* (**b**, **d**) expression during the duration of IFN-α2a treatment in the IFN-α2a group alone (**a**, **b**) and during infection in the IFN-α2a ($n = 6$) and placebo ($n = 9$) groups (**c**, **d**). *P* values were calculated by Wilcoxon matched pairs signed rank test. **e**, Percentage of *in vitro* IFN antiviral activity inhibited by plasma from IFN-α2a ($n = 6$) and placebo ($n = 3$) macaques. **f**, Expression of *FOXO3a* and FOXO3a-bound genes in SIV-uninfected macaques ($n = 3$) treated with 21 days of IFN-α2a. Large circles indicate statistically significant ($P<0.05$) changes from pre-IFN-α2a treatment calculated by Wilcoxon matched pairs signed rank test. Small circles indicate no statistically significant change from pre-IFN-α2a treatment. **g**, Expression of IFN-α-regulatory genes in IFN-α2a ($n = 6$) and placebo ($n = 9$) macaques. *P* values represent the comparison between FPKMs of IFN-α2a ($n = 6$) and placebo ($n = 9$) macaques at 7 d.p.i. **h**, Expression of FOXO3a-bound genes in IFN-α2a (green, $n = 6$) and placebo (blue, $n = 9$) macaques at 7 d.p.i.

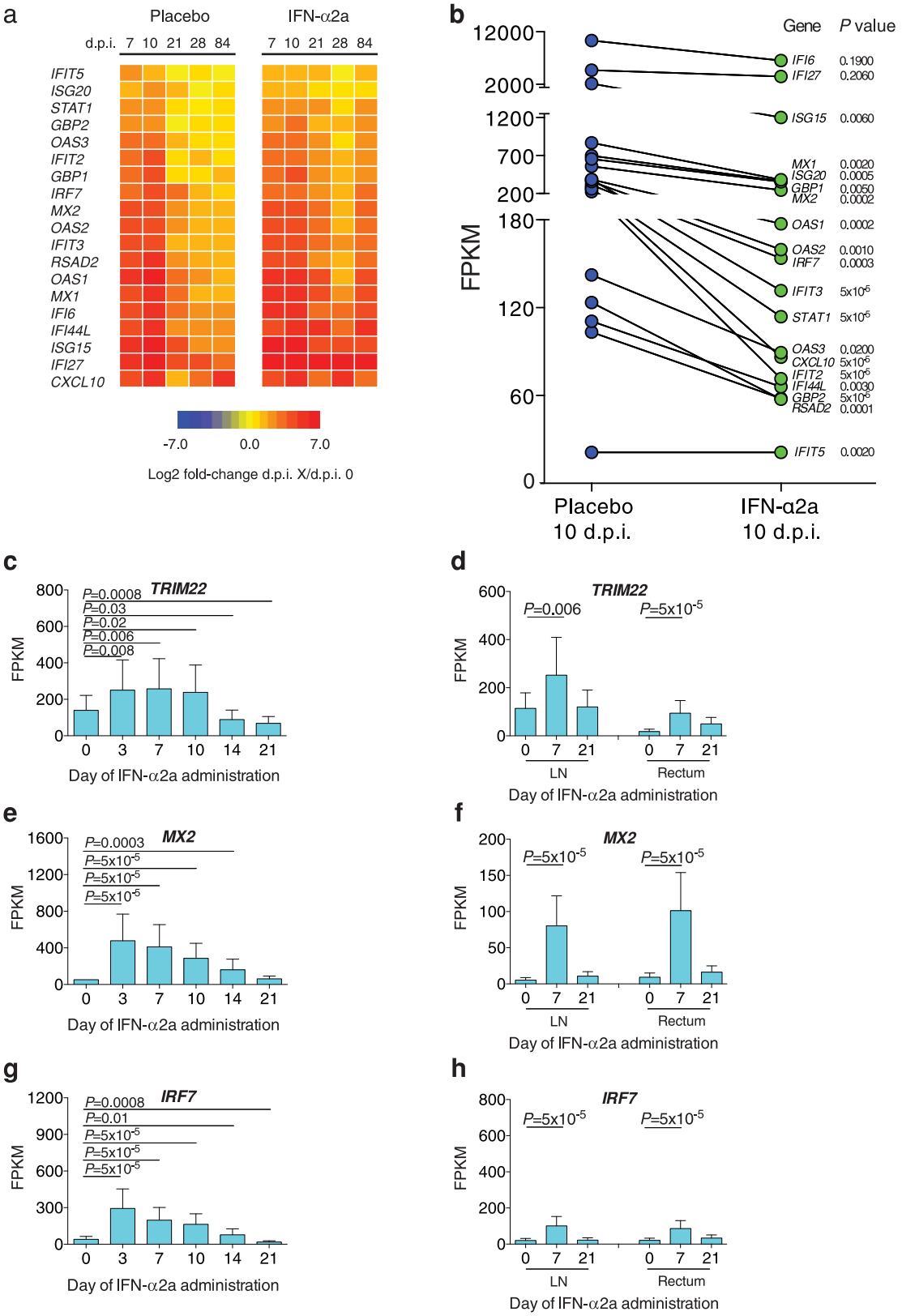

Extended Data Figure 7 | Effects of IFN-α2a on IFN-stimulated and antiviral genes. **a**, ISGs in PBMCs in IFN-α2a ($n = 6$) and placebo ($n = 9$) macaques. Red indicates upregulation, yellow indicates no change and blue indicates downregulation relative to pre-infection. **b**, Expression of ISGs in macaques treated with IFN-α2a ($n = 6$) or placebo ($n = 9$). *P* values indicate differentially expressed genes at 10 d.p.i. **c–h**, Expression of *TRIM22* (**c**, **d**), *MX2* (**e**, **f**) and *IRF7* (**g**, **h**) in SIV-uninfected macaques ($n = 3$) treated with weekly IFN-α2a for 3 weeks in PBMCs (**c**, **e**, **g**) and lymph nodes and rectum (**d**, **f**, **h**). Day 0 reflects baseline. Numbers indicate days since first IFN-α2a administration. Error bars indicate range. *P* values were calculated by Wilcoxon matched pairs signed rank test.

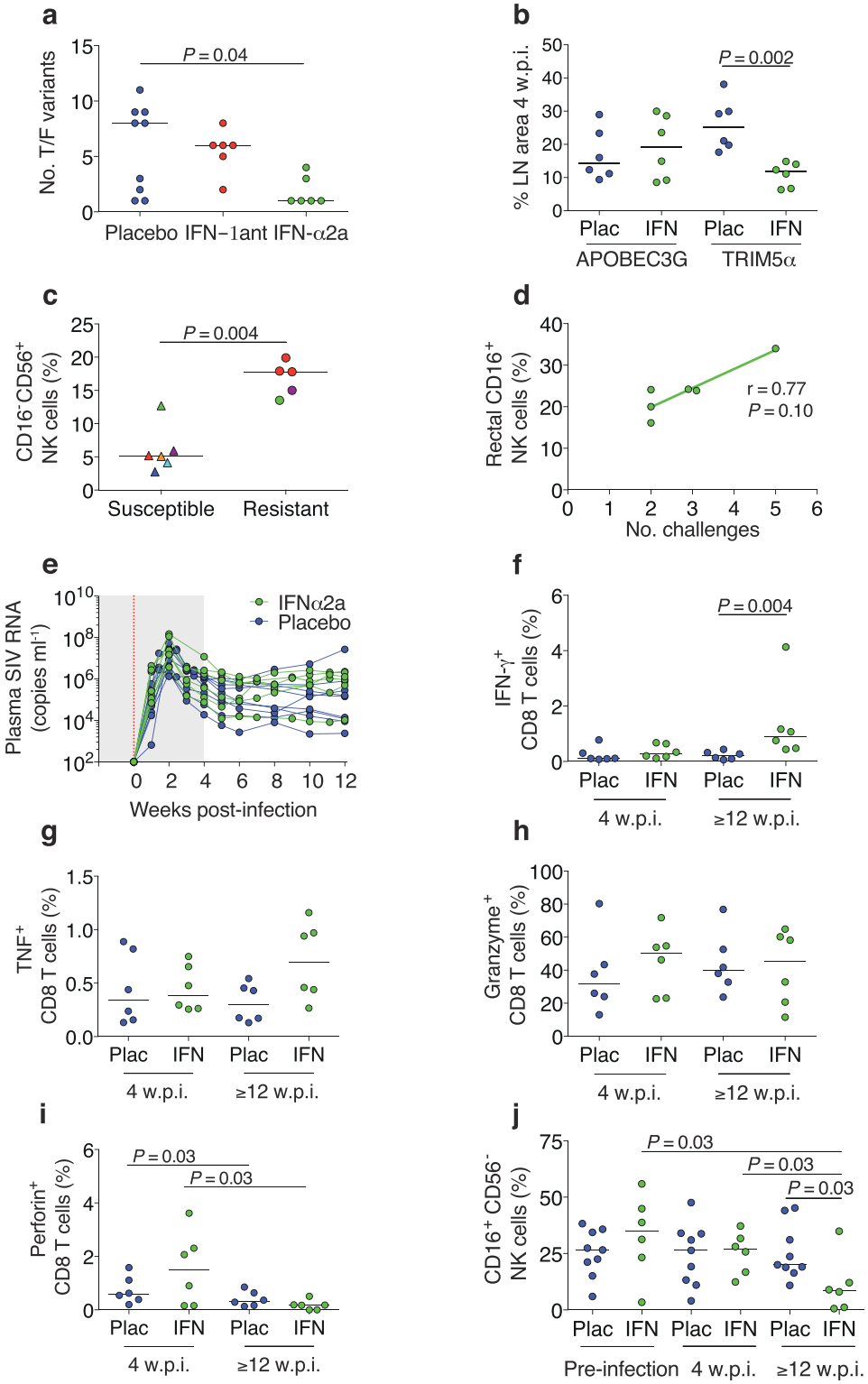

Extended Data Figure 8 | Effects of IFN-α2a on SIV control. **a**, Number of transmitted/founder (T/F) variants in placebo ($n = 9$), IFN-1ant ($n = 6$) and IFN-α2a ($n = 6$) macaques. *P* value was calculated by Mann–Whitney *U* test. **b**, Antiviral protein production in lymph nodes (LN) by immunohistochemistry at 4 w.p.i. in IFN-α2a ($n = 6$) and placebo ($n = 6$) macaques. *P* value was calculated by Mann–Whitney *U* test. **c**, $CD56^+$ NK-cell frequency on the day of challenge stratified by whether the macaque resisted or was susceptible to systemic infection that day. Each IFN-α2a macaque ($n = 6$) is indicated by a different colour. Circles indicate that the macaque was resistant to infection with the next challenge and triangles indicate that the macaque was susceptible to infection with the next challenge. *P* value was calculated by Mann–Whitney *U* test. **d**, Correlation between the number of challenges required to achieve systemic infection and rectal $CD16^+$ NK-cell frequency in each macaque ($n = 6$) at 4 w.p.i. *r* indicates the Spearman's rank correlation coefficient. *P* value indicates the significance of the correlation. **e**, Plasma SIV RNA levels in macaques treated with IFN-α2a ($n = 6$) or placebo ($n = 9$) saline. Shading reflects treatment period. Red vertical line indicates day 0 of systemic SIV infection. **f–i**, Frequency of IFN-γ^+ (**f**), TNF^+ (**g**), granzyme B^+ (**h**) and $perforin^+$ (**i**) CD8 T cells at 4 and ≥12 w.p.i. in IFN-α2a ($n = 6$) and placebo ($n = 6$) macaques. **j**, Frequency of circulating $CD16^+CD56^-$ NK cells in IFN-α2a ($n = 6$) and placebo ($n = 9$) macaques. *P* values at different time points within treatment groups were calculated by Wilcoxon matched pairs signed rank test and between groups by Mann–Whitney *U* test.

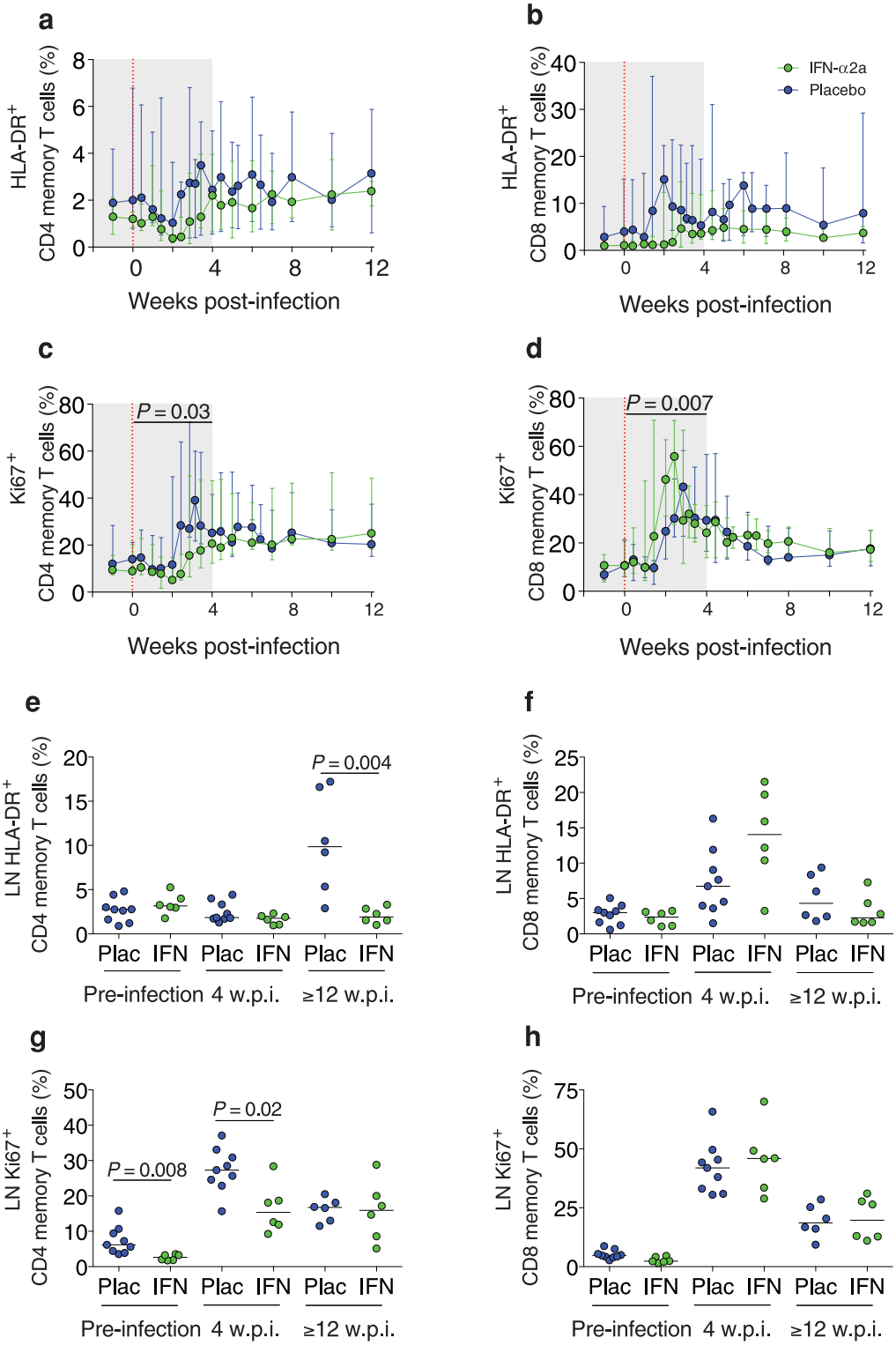

Extended Data Figure 9 | Effects of IFN-α2a on T-cell activation. **a**–**h**, Frequency of peripheral blood (**a**–**d**) and lymph node (LN) (**e**–**h**) CD4 (**a**, **c**, **e**, **g**) and CD8 (**b**, **d**, **f**, **h**) memory T cells expressing HLA-DR (**a**, **b**, **e**, **f**) or Ki67 (**c**, **d**, **g**, **h**) in IFN-α2a (IFN, $n = 6$) and placebo (Plac, $n = 9$) macaques. Shading indicates treatment period. Error bars indicate range. **a**–**d**, Red vertical line indicates day 0 of systemic SIV infection. *P* values represent the comparison between groups of the AUC (0-4 w.p.i.). **e**–**h**, Horizontal bars indicate median values. *P* values were calculated by Mann–Whitney *U* test.

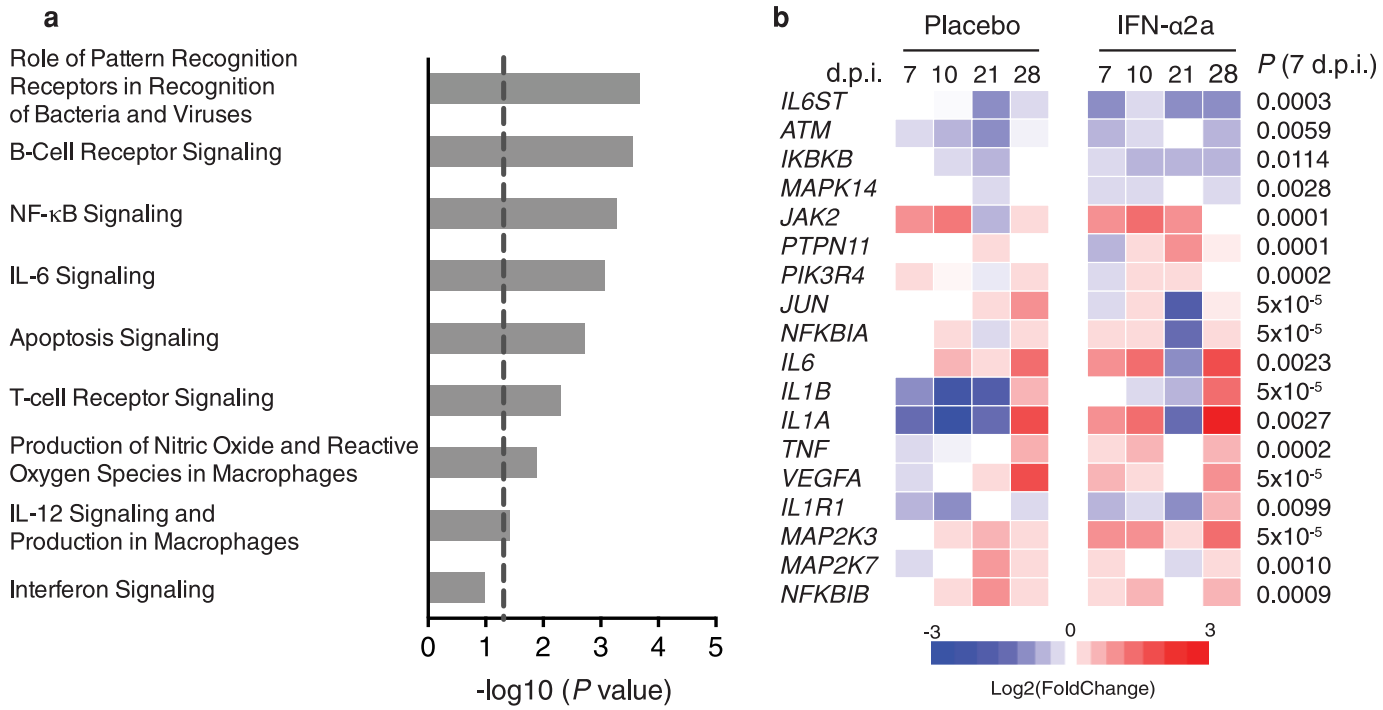

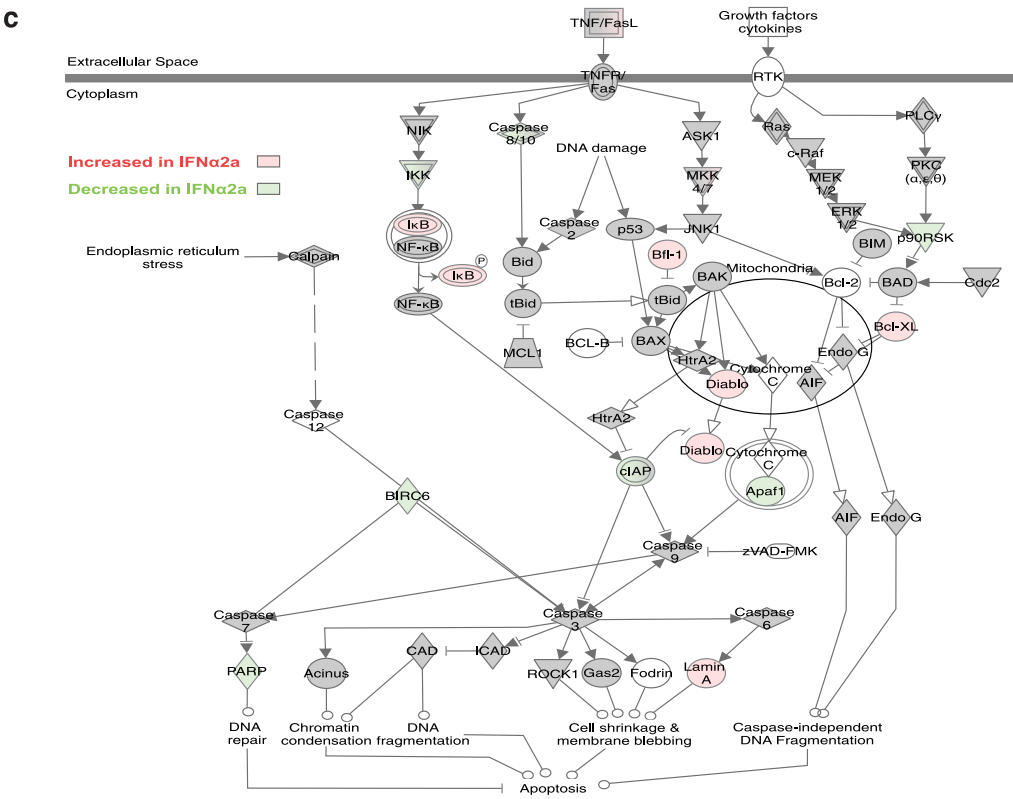

Extended Data Figure 10 | Effects of IFN-α2a on gene expression. **a**, Selected pathways significantly affected by IFN-α2a treatment. *P* values were calculated by Fisher's exact test with the Benjamini–Hochberg multiple testing correction. **b**, Expression of genes downstream of IL-6 signalling. Upregulation relative to before IFN-α2a or placebo treatment and SIV infection is represented by red, no change by white, downregulation by blue. *P* values represent the comparison between IFN-α2a ($n = 6$) and placebo ($n = 9$) macaques at 7 d.p.i. **c**, Selected genes in apoptosis signalling pathways. Significant upregulation at 7 d.p.i. is represented by red, downregulation by green.